

University of Dundee

Effects of screw pile installation on installation requirements and in-service performance using the Discrete Element Method

Sharif, Yaseen Umar; Brown, Michael John; Cerfontaine, Benjamin; Davidson, Craig; Ciantia, Matteo Oryem; Knappett, Jonathan Adam

Published in:
Canadian Geotechnical Journal

DOI:
[10.1139/cgj-2020-0241](https://doi.org/10.1139/cgj-2020-0241)

Publication date:
2021

Document Version
Peer reviewed version

[Link to publication in Discovery Research Portal](#)

Citation for published version (APA):

Sharif, Y. U., Brown, M. J., Cerfontaine, B., Davidson, C., Ciantia, M. O., Knappett, J. A., Brennan, A., Ball, J. D., Augarde, C., Coombs, W. M., Blake, A., Richards, D., White, D., Huisman, M., & Ottolini, M. (2021). Effects of screw pile installation on installation requirements and in-service performance using the Discrete Element Method. *Canadian Geotechnical Journal*, 58(9), 1334-1350. <https://doi.org/10.1139/cgj-2020-0241>

General rights

Copyright and moral rights for the publications made accessible in Discovery Research Portal are retained by the authors and/or other copyright owners and it is a condition of accessing publications that users recognise and abide by the legal requirements associated with these rights.

- Users may download and print one copy of any publication from Discovery Research Portal for the purpose of private study or research.
- You may not further distribute the material or use it for any profit-making activity or commercial gain.
- You may freely distribute the URL identifying the publication in the public portal.

Take down policy

If you believe that this document breaches copyright please contact us providing details, and we will remove access to the work immediately and investigate your claim.

Effects of screw pile installation on installation requirements and in-service performance using the Discrete Element Method

Journal:	<i>Canadian Geotechnical Journal</i>
Manuscript ID	cgj-2020-0241.R3
Manuscript Type:	Article
Date Submitted by the Author:	n/a
Complete List of Authors:	Sharif, Yaseen; University of Dundee, School of Science and Engineering Brown, Michael; University of Dundee Cerfontaine, Benjamin; University of Dundee, Civil Engineering Davidson, Craig; University of Dundee, School of Science and Engineering Ciantia, Matteo; University of Dundee, Knappett, Jonathan; University of Dundee, Civil Engineering Ball, Jonathan; Roger Bullivant Ltd Brennan, Andrew; University of Dundee Augarde, Charles; Durham University, School of Engineering and Computing Science Coombs, William; Durham University, Department of Engineering Blake, Anthony; University of Southampton Faculty of Engineering and the Environment Richards, David; University of Southampton White, David; University of Southampton Faculty of Engineering and the Environment, Faculty of Engineering and Physical Sciences Huisman, Marco; Heerema Marine Contractors Ottolini, Marius; Heerema Marine Contractors
Keyword:	Installation Effects, Screw Piles, Discrete element method, Silent Piling
Is the invited manuscript for consideration in a Special Issue? :	Not applicable (regular submission)

SCHOLARONE™
Manuscripts

Date of 3rd revised submission 12/10/2020

Date of 2nd revised submission 27/08/2020

Date of 1st revised submission 10/07/2020

Date of original submission: 16/04/2020

Title

Effects of screw pile installation on installation requirements and in-service performance using the Discrete Element Method

Author list

Yaseen Umar Sharif*, Michael John Brown, Benjamin Cerfontaine, Craig Davidson, Matteo Oryem Ciantia, Jonathan Knappett, Andrew Brennan, Jonathan David Ball, Charles Augarde, William Coombs, Anthony Blake, David Richards, David White, Marco Huisman and Marius Ottolini

**Corresponding author*

Author details

Yaseen Umar Sharif, MEng

PhD student, School of Science and Engineering, University of Dundee, Fulton Building, Dundee, DD1 4HN, UK

ORCID: 0000-0002-3620-7500

Email: y.u.sharif@dundee.ac.uk

Michael John Brown, BEng PhD GMICE

Reader, School of Science and Engineering, University of Dundee, Fulton Building, Dundee, DD1 4HN, UK

ORCID: 0000-0001-6770-4836

Email: m.j.z.brown@dundee.ac.uk

Benjamin Cerfontaine, BSc, MSc, PhD

MSCA Research Fellow, School of Science and Engineering, University of Dundee, Fulton Building, Dundee, DD1 4HN, UK

ORCID: 0000-0002-4833-9412

Email: b.cerfontaine@dundee.ac.uk

Craig Davidson, BSc MSc

Research Associate, School of Science and Engineering, University of Dundee, Fulton Building, Dundee, DD1 4HN, UK

ORCID: 0000-0002-4843-5498

Email: c.s.davidson@dundee.ac.uk

Matteo Oryem Ciantia,

Lecturer, School of Science and Engineering, University of Dundee, Fulton Building, Dundee, DD1 4HN, UK

ORCID: 0000-0003-1897-4471

Email: m.o.ciantia@dundee.ac.uk

Jonathan Adam Knappett, MEng (Hons), PhD

Professor of Civil Engineering, School of Science and Engineering, University of Dundee, Fulton Building, Dundee, DD1 4HN, UK

ORCID: 0000-0003-1936-881X

Email: j.a.knappett@dundee.ac.uk

Jonathan David Ball, BSc, CGeol, FGS

Chief Geotechnical Engineer, Roger Bullivant Ltd, Burton Upon Trent, UK

Email: Jon.Ball@roger-bullivant.co.uk

Andrew Brennan, MEng PhD GMICE

Senior Lecturer, School of Science and Engineering, University of Dundee, Fulton Building,
Dundee, DD1 4HN, UK

ORCID: 0000-0002-8322-0126

Email: a.j.brennan@dundee.ac.uk

Charles Augarde, BSc MSc DPhil CEng FICE

Professor, Department of Engineering, Durham University, Durham, DH1 3LE, UK

ORCID: 0000-0002-5576-7853

Email: charles.augarde@durham.ac.uk

Will Coombs, MEng PhD

Associate Professor, Department of Engineering, Durham University, Durham, DH1 3LE, UK

ORCID: 0000-0003-2099-1676

Email: w.m.coombs@durham.ac.uk

Anthony Blake, BEng, PhD

Research Fellow, Faculty of Engineering and the Environment, University of Southampton, SO17
1BJ, UK

ORCID: 0000-0001-5718-7900

Email: a.p.blake@soton.ac.uk

David Richards, BEng MSc PhD CEng MICE

Professor, Faculty of Engineering and the Environment, University of Southampton, UK

ORCID: 0000-0002-3819-7297

Email: [dj@r@soton.ac.uk](mailto:djr@soton.ac.uk)

David White, MA, MEng, PhD, FEng, FTSE, FRINA, FIEAust

Professor, Faculty of Engineering and the Environment, University of Southampton, UK

ORCID: 0000-0002-2968-582X

Email: david.white@soton.ac.uk

Marco Huisman, MSc PhD

Technology advisor, Heerema Marine Contractors, Leiden, the Netherlands

ORCID: 0000-0001-9704-5843

Email: mhuisman@hmc-heerema.com

Marius Ottolini, MSc

Heerema Marine Contractors, Leiden, the Netherlands

ORCID: 0000-0003-4596-0016

Email: mottolini@hmc-heerema.com

Main text word count: 9179

Number of tables: 2

Number of Figures: 14

Effects of screw pile installation on installation requirements and in-service performance using the Discrete Element Method

Author list

Yaseen Umar Sharif, Michael John Brown, Benjamin Cerfontaine, Craig Davidson, Matteo Oryem Ciantia Jonathan Knappett, Andrew Brennan, Jonathan David Ball, Charles Augarde, William Coombs, Anthony Blake, David Richards, David White, Marco Huisman and Marius Ottolini

Abstract

Existing guidance on the installation of screw piles suggest that they should be installed in a pitch-matched manner to avoid disturbance to the soil which may have a detrimental effect on the in-service performance of the pile. Recent insights from centrifuge modelling have shown that installing screw piles in this way requires large vertical compressive (or crowd) forces, which is inconsistent with the common assumption that screw piles pull themselves into the ground requiring minimal vertical compressive force. In this paper, through the use of the Discrete Element Method (DEM), the effects of advancement ratio, i.e. the ratio between the vertical displacement per rotation to the geometric pitch of the helix of the screw pile helix, on the installation resistance and in-service capacity of a screw pile is investigated. The findings are further used to assess the applicability of empirical torque capacity correlation factors for large diameter screw piles. The results of the investigation show that it is possible to reduce the required vertical compressive installation force by 96% by reducing the advancement ratio and that although over-fighting a screw pile can decrease the subsequent compressive capacity, it appears to increase the tensile capacity significantly.

Keywords: Installation Effects, Screw Piles, Discrete element method

1 Introduction

A screw pile is a form of displacement pile, which consist of a central steel shaft with one or more helices welded to the shaft at specific intervals (Lutenegger and Tsuha, 2015) (Figure 1). Existing industrial guidance on the installation of screw piles suggests that screw piles should be installed in a pitch-matched manner (Perko 2009; BS8004 2015) to avoid disturbance to the soil that will then have a detrimental effect on post installation pile capacity. This may be for either tension or compression loading. Pitch-matched, or 'perfect', installation refers to a rate of vertical advancement of the pile per rotation, that corresponds to the distance between the helix leading edge and the end of the helix (Figure 1a). Perfect or pitch-matched installation would therefore result in an advancement ratio (AR) of 1 (Bradshaw *et al.* 2019) where the advancement ratio is defined as:

$$AR = \frac{\Delta z}{P_h} \quad (1)$$

where Δz is the vertical displacement per rotation and P_h is the geometric pitch of the helical plate. Within the codification of such approaches (BS8004 2015) it is normal to allow under-flighting ($AR > 1$) or over-flighting ($AR < 1$) by up to about 20% (i.e. $AR = 0.8-1.2$) but it is unclear what such variation in control would have on installation requirements and the final in-service performance of the pile. If deep foundations with similar installation methods, such as continuous flight augers (*CFA*) are considered, a different approach to the advancement ratio is adopted, which is designed to cause the least amount of disturbance during installation. Viggiani (1989) states that the ideal advancement ratio for *CFA*, to minimise disturbance, is dependent upon the geometry of the auger and is defined as

$$v_{crit} = n P_h \left(1 - \frac{D_c^2}{D_h^2} \right) \quad (2)$$

where v_{crit} is the critical drilling velocity, n is the rate of revolution, D_h is the diameter of the helix, and D_c is the diameter of the central core of the pile (or shaft section). Equation 2 is based on equating the volume of soil displaced by the pile to the volume of soil removed. This is likely to minimise the change in stress of the soil surrounding the auger during its installation. If the vertical velocity is greater than v_{crit} a net compression effect below the helices is produced, increasing the vertical installation force and torque.

Shi *et al.* (2019) investigated the effect of critical drilling velocity on the installation requirements of multi helix complex screw pile geometries using 1g physical modelling and the Discrete Element Method (DEM). The results of their investigation show that a change in particle displacement and therefore mechanism occurs when installing above and below v_{crit} . Shi *et al.* (2019) showed that it is possible to reduce both the compressive installation force and torque of the screw pile by decreasing the vertical velocity (by 50%) or in other words decreasing the advancement ratio (AR). However, they do not comment on the post installation in-service performance of the installed pile. It is also anecdotally assumed that a screw pile will screw itself into the ground if rotated under its own self-weight but if this is the installation mechanism it is unclear how it would be possible to maintain a constant $AR = 1$ and overcome the installation resistance, as required in BS8004:2015. Bradshaw *et al.* (2019) has shown that when installing a screw pile under its own self weight an AR of 0.5 is typically achieved, much lower than the pitch-matched guidance. Similarly when attempting to install screw piles at $AR = 1.0$ during field testing, Richards *et al.* (2019) found that they were unable to do so using conventional installation equipment due to the excessive vertical force that was required. Instead, the monitored AR typically ranged between 0.8 and 0.5, which is below the recommended range of 0.8-1.2.

The immediately apparent way to investigate this issue further would be to look at the many screw pile installations undertaken to date by industry. Unfortunately, though, screw pile rigs very rarely record installation rates (AR) or measure torque directly, although it is often inferred indirectly from

hydraulic pump pressures. Applied vertical force or “crowd” is also not recorded therefore it is very difficult to investigate the effects of installation from current practice.

Part of the motivation for investigating screw pile installation has been the development of silent offshore piling techniques for renewable energy deployment, and in particular as an alternative foundation type for offshore wind and floating future wind (Davidson *et al.* 2019, 2020). To achieve this, significant upscaling of typical onshore screw piles is required, resulting in quite different geometry. Davidson *et al.* (2019) showed that screw piles capable of supporting a typical four-legged offshore jacket structure would require significant installation torque to install (7MNm) and very high vertical compressive forces to achieve pitch-matched installation (23MN). As part of this work an insitu cone penetration test (*CPT*) method was developed to allow prediction of both installation torque and crowd for various geometries of screw piles with pitch-matched installation (Davidson *et al.*, 2018, 2020).

On attempting to validate this method against the results of other onshore studies (Gavin *et al.* 2013) it was found that the torque predictions performed well but the measured and predicted crowd forces were much larger than could be achieved by the rigs used to install them if a pitch matched approach was used. As the screw piles had been installed successfully therefore there was either a flaw in the prediction methods developed or the piles were not installed in a pitch-matched fashion as prescribed. On further investigation it was found that generally onshore screw pile rigs had high torque capabilities but relatively low self-weights suggesting large crowd forces are not encountered or applied in the field. Therefore, it was decided to investigate the effects of over flighting or under flighting on screw pile installation requirements and in-service capacity using the Discrete Element Method (*DEM*). The aim is firstly to resolve whether a lower AR is the likely explanation for high crowd forces not being needed in practice, and secondly to assess the resulting effect of AR on the subsequent vertical capacity.

The *DEM* technique has been successfully used previously to investigate penetration events e.g. insitu soil characterisation, pile installation behaviour and screw pile installation, based upon calibration against centrifuge tests and triaxial testing (Butlanska *et al.* 2014; Ciantia *et al.* 2016; Duan *et al.* 2018; Sharif *et al.* 2019a; Zhang *et al.* 2019).

An additional motivation for the study was to investigate the empirical relationship that is often adopted in practice between torque and pile capacity. It is often suggested that the torque required to install a screw pile can be predicted based upon a unique factor (K_t or K_c for tension and compression respectively) that relates the observed installation torque to pile capacity (Hoyt and Clemence 1989; Perko 2009; Tsuha and Aoki 2010; Byrne and Houlsby 2015; Houlsby 2016). When using K_t or K_c to predict the installation torque, the pile capacity is typically is determined based upon published empirical techniques (Perko 2009; Das and Shukla 2013). It has also been proposed that the same torque relation factor (K) can be used in tension and compression, which is calculated based upon the diameter of the screw pile core (Perko 2009):

$$Q_t = TK_t \quad (3)$$

where Q_t is the axial tensile capacity of a screw pile and T is the installation torque at the end of installation. Perko (2009) related the K factor to the diameter of the pile central core (D_c) by fitting the following equation to model and field experiments:

$$K = 2.54D_c^{-0.9198} \quad (4)$$

where the units of D_c and K are m and m^{-1} respectively. Byrne and Houlsby (2015) and Houlsby (2016) developed a dimensionless torque factor (K_t^*) by including the helix diameter (D_h).

$$Q_t = \frac{TK_t^*}{D_h} \quad (5)$$

These authors suggested that K_t^* should tend towards a value between 8 and 10. However, on inspection of the data used by Perko (2009) to define this relationship it is apparent that there is significant scatter in the data set and that only a limited range of pile core diameters were used

which are far below those which may be required for offshore deployment (Davidson *et al.* 2020). Lutenegger (2013) suggested that it may be incorrect to assume that a single parameter model works effectively for all screw pile configurations and soils as suggested by equations (4) and (5). He also suggested that correlations are often the same whether one or two helices are included. Lutenegger (2019) states that where Hoyt and Clemence (1989) compared results of a large number of field tension load tests in different soils the accuracy between observed and calculated values (expressed as the ratio of measured to computed capacity) ranged from approximately 0.3 to 4.5, suggesting considerable scatter in any individual value of K_t adopted. Lutenegger (2019) also suggested that this approach is sensitive to pile geometry and number of helix plates but does not comment on the effects of the installation approach (e.g. *AR*).

In this paper the effects of advancement ratio on the installation requirements and axial performance of a single screw pile geometry installed in sand of different relative densities is investigated using the Discrete Element Method. The results are used to investigate the effect of advancement ratio on installation requirements, the resulting vertical load capacity and the applicability of the empirical torque capacity correlation factors K_t , K_t^* , K_c and K_c^* for larger diameter screw piles.

2 Method adopted for DEM modelling and pile details

The Discrete Element Method (*DEM*) is a numerical modelling framework which can be used to simulate large deformation problems in granular soils (Ciantia *et al.* 2019). Rather than using a continuum to model the soil, *DEM* uses discrete particles that have the ability to interact as a soil body. With the application of an increased gravitational field, the *DEM* is able to act as a virtual centrifuge (Ciantia *et al.* 2018; Sharif, *et al.* 2019a) when properly calibrated (as detailed in Sharif *et al.* (2019a)), with the added benefit of using a single soil bed (particle arrangement) which can be reset and used multiple times (Shi *et al.* 2019).

139 To model the installation of the large diameter plugged screw piles, Particle Flow Code 3D 5.0.35
140 (Itasca Consulting Group 2016) was used alongside a simplified Hertz-Mindlin contact model
141 (Mindlin and Deresiewicz 1953) , in which the contact stiffness is modelled using non liner springs.
142 Spherical particles are used with the rotation of the particles inhibited to capture the rotational
143 resistance of angular grains (Arroyo *et al.* 2011; Ciantia *et al.* 2019). Viscous damping is not used in
144 either of the contact models, as the simulation occurs under drained and no viscosity is needed. The
145 critical damping was also set to 0 as the simulation is conducted under quasi-static conditions. The
146 parameters for the particle -particle contact model were calibrated against laboratory triaxial tests
147 conducted at a confining pressure of 60kPa, and at relative densities of 30% and 70% in order to
148 capture both the peak and residual response of the soil. The *DEM* implementation of the triaxial
149 tests used representative element volumes (*REV*), which consist of a small cluster of around 5000
150 particles (cube with sides of 2.5mm) consolidated to the required relative densities under a confining
151 pressure of 60kPa using a stress controlled servo on all boundaries. Using *REV*s during the calibration
152 process, allowed for many iterations of the contact parameters to be tested to determine the values
153 that best reproduced the laboratory results. During shearing of the *REV*, the stress control servo was
154 maintained on the lateral boundaries at 60kPa, while the bottom boundary was fixed, and the top
155 boundary was displaced using strain-control.

156 For each change in contact model parameters, a new *REV* was created, tested and compared to the
157 physical results. The shear modulus (*G*) and the Poisson's ratio (*v*) were kept constant at 3GPa and
158 0.3 respectively and the interparticle friction (μ) was varied for each of the *DEM* triaxial tests
159 conducted. Particle rotation was inhibited in all simulations to capture the rotational resistance of
160 angular grains (Arroyo *et al.* 2011). A μ of 0.264 was able to reproduce the laboratory results (Sharif
161 *et al.* 2019a) and match the peak response of the soil, although the residual soil strength is slightly
162 higher than that of the laboratory tests. This value represents the frictional resistance between two
163 individual particles and not the soil body as a whole with none rotating particles and therefore does
164 not equate to a classical friction angle.

Once the particle-particle contact model parameters had been determined the particle-structure contact model was calibrated against data obtained through centrifuge testing of straight shafted piles (Al-Baghdadi 2017). A soil bed with the same boundary conditions and dimensions as the centrifuge test was created, using the soil-soil contact model calibrated against the triaxial tests. A straight shafted pile of diameter 0.5m and length 10m was then installed into the soil bed using two methods. The first method was a monotonic push (i.e. no rotation of the pile) and the second method was using a rotary installation at the same rotation rate as per Al-Baghdadi (2017). The shear modulus (G_{pile}) and the Poisson's ratio (ν_{pile}) were kept constant at 3GPa and 0.3 respectively and the interface friction coefficient (μ_{pile}) was modified in order to match the compressive installation force and the installation torque reported from the centrifuge experiments. For each alteration of the contact model parameters, the soil bed was reset, and the simulation repeated with the new the parameters. Through this iterative process the interface friction coefficient was found to be 0.16 (Sharif *et al.* 2019a). The interface friction coefficient may appear lower than expected for physical model tests. This is due to the value representing the interaction of a single spherical particle on the surface of the pile with, with the rotation of the particle being restricted in order to model the rolling resistance of the angular soil particle.

The calibrated contact models were further validated, by modelling the pitch-matched installation of the O2VD screw pile from Davidson *et al.* (2019). The O2VD screw pile is a dual helix screw pile, with an optimised central core (lower shaft has a smaller diameter than the upper shaft) and is drastically different to that of the straight shafted pile used for the previously described calibration purposes. Sharif *et al.* (2019a) showed that the contact models were able to accurately reproduce both the installation torque and the compressive installation force from the centrifuge tests. Further validation can be seen in Figure 5e and 5f, in which the centrifuge axial response of the pitch-matched U1VDB pile (Davidson *et al.* 2020) is compared to the *DEM* results of this study. From Figure 5f the tensile uplift response of the centrifuge tests on the pitch matched U1VDB pile has been included, The *DEM* simulation is able to match the general trend of the centrifuge results,

although the measured force is slightly lower in the DEM model than in the physical test. From Figure 5e, the DEM is shown to replicate the load displacement curve of the pitch matched centrifuge axial compressive test accurately. Further validating the contact models used within this study and how they are able to capture the characteristics of the soil being modelled. Further details on the calibration and validation of the contact models used within this study can be found in Sharif *et al.* (2019a,b). These are outlined in Table 1 (Sharif *et al.* 2019a).

The sand modelled in the simulations is based upon the properties of HST95, which is a medium to fine well-graded sand that is commonly used at the University of Dundee in physical modelling (Davidson *et al.* 2019) and element testing. The particle size distribution (*PSD*) is the same as that of HST95 sand (see Table 1) and can be seen in Lauder (2010). The behaviour and properties of the soil have been previously investigated and are well documented (Al-Defae *et al.* 2013; Lauder *et al.* 2013).

The virtual soil beds for DEM analysis were created in accordance with the specification in Sharif *et al.* (2019b). Three soil beds were created using the periodic cell replication method (Ciantia *et al.* 2018) and particle refinement method (McDowell *et al.* 2012), with each bed having a different relative density (D_r), based upon the physical voids ratio of the sand modelled. The relative densities selected were 30%, 52% and 83%, with the densest bed being consistent with the physical modelling study conducted by Davidson *et al.* (2019). The soil beds used had a diameter of 40m (0.5m) and a height of 32m (0.4m) (Table 2), frictionless rigid boundaries were present at the base of the soil bed and surrounding the circumference. This resulted in the lateral and bottom boundaries having a fixed condition, with the top boundary being free. Additional properties of the beds can be seen in Table 2.. To avoid any boundary effects, the radius of the soil bed was made to be greater than the $20R$ as suggested by Bolton *et al.* (1999), where R in this particular case is the radius of the pile helix (i.e. the largest radius of the pile). This is supported by the finding of Sharif *et al.* (2020) who showed that there was negligible increase in mean effective stress at a radial distance of $13R$ and no increase

at a radial distance of $20R$ when installing piles using the DEM. Additional information and detail of the formation process can be found in Sharif *et al.* (2019b) and Ciantia *et al.* (2018).

To reduce the run-time of the simulation, a particle size distribution (*PSD*) scaling value (n_i) of 20 was used at the centre of the sample with a maximum n_i of 96.5 at the boundaries. This value represents the multiplier applied to the diameter of particles, so that each particle represented n_i^3 particles with the bulk properties of the soil remaining the same. This methodology has previously been implemented by McDowell *et al.* (2012) and Shi *et al.* (2019). The particle scaling of 20 was selected based upon the minimum recommended ratio of diameter of the pile core (D_c) to the median particle size (d_{50}) of 2.69 (Arroyo *et al.* 2011). It is also imperative that the screw pile pitch (P_h) is considered when selecting the particle scaling, to avoid causing a blockage of particles in the helix opening. A minimum ratio of the helix pitch to the maximum particle size (d_{100}) of 2.5 was implemented for this study. This typically results in an average of 15 to 17 particles passing through the helix pitch at any given moment (Figure 2). An example soil bed can be seen in Figure 2. Where the shading of the particles represents different values of n_i . To limit the possibility of particle migration between scaling zones, the increase in the *PSD* scaling value (n_i), between adjacent concentric zones, is limited to 1.3 for this soil type, such that the smallest particle (d_{00}) of the larger scale is smaller than the median particle in the smaller scale. This ratio is much smaller than that proposed by Terzaghi (1939) and should therefore limit the possibility of particles with different values of n_i merging together. Further details on soil bed formation and particle scaling criteria are outlined in Sharif *et al.* (2019b). The gravitational field applied to the soil bed was set at 48g to match the dry sand centrifuge tests of Davidson *et al.* (2019) which actually represented the effective stress within a saturated prototype scale of 80 after the method developed by Li *et al.* (2010) and validated by Klinkvort *et al.* (2013). The calculated results from the simulations were scaled in accordance with centrifuge scaling laws (Garnier *et al.* 2007), such that the length is multiplied by N , force by N^2 and torque by N^3 , where N is the model scaling factor ($N=80$)

Frictional rigid boundaries (walls) were used to model the geometry of the pile. The geometry of the screw pile used in this study is based upon the U1VDB screw pile used in the centrifuge study conducted by Davidson *et al.* (2019). The geometry selected in this research is based upon the findings of the optimisation studies of Knappett *et al.* (2014), Al-Baghdadi (2017) and Davidson *et al.* (2019). The pile has model (and prototype) dimensions as follows: core diameter (D_c) of 11mm (0.88m), a helix diameter (D_h) of 21.25mm (1.7m), a length (L) of 160mm (12.8m) and a helix pitch (P_h) of 7mm (0.56m), (Figure 1b). This results in a pile with a relatively shallow embedment depth ($H/D_h = 7$) and according to Equations 1 and 2 (Viggiani 1989) a critical advancement ratio of 0.72 for volume balance, which lies outside of the recommended 20% variation on advancement ratio for screw piles (BS8004 2015). Due to the size of the particles relative to the core diameter used in both the centrifuge tests and the DEM simulations the piles used within these studies have been modelled as closed-ended piles.

To determine the installation rate of the pile, for both vertical and rotational velocities, and to produce a quasi-static state, a fixed the inertial number (I) was used. The inertial number is used to define the point at which dynamic effects occur under shearing (da Cruz *et al.* 2005). To determine the limiting value for the inertial number, a sensitivity analysis was conducted, in which the compressive installation force of a pile installed at different velocities were compared. The velocities chosen result in an inertial number of 0.001, 0.01, 0.05 and 0.1. The sensitivity analysis resulted in a value of 0.01 being chosen as values higher than this resulted in an increase in compressive installation forces. The limiting value of 0.01 has been used in previous *DEM* studies to investigate pile penetration problems (Janda and Ooi 2016; Ciantia *et al.* 2019; Martinez *et al.* 2020). This value was then used to calculate the vertical and rotational velocity of the pile using Equations 6 to 9.

$$I = \dot{\gamma} d_{50} \sqrt{\rho / p_0'} \quad (6)$$

$$\dot{\omega} = \dot{\gamma} L_{pv} \quad (7)$$

$$\dot{\theta} = \dot{\gamma} L_{pr} \frac{2\pi}{D_h} \quad (8)$$

$$AR = \frac{2\pi \dot{w}}{\dot{\theta} P_h} \quad (9)$$

where $\dot{\gamma}$ is the shear strain rate, p_o' is the mean effective stress at the depth of penetration, ρ is the density of the particles, d_{50} is the median particle size in the region of penetration (core of the sample), \dot{w} is the vertical velocity in m/s, $\dot{\theta}$ is the rotational velocity in rad/s, P_h is the geometric pitch of the helix and L_p is the width of the plastic deformation zone, as discussed below.

The widths of the plastic deformation zone (L_p) for the vertical velocity (L_{pv}) and rotational velocities (L_{pr}) were assumed to be $3D_h$ and $4D_h$, respectively. Previous studies on the installation of straight shafted piles (Lu *et al.* 2004; Garcia - Galindo *et al.* 2018) have shown that different shearing mechanism occur when installing a straight shafted pile using rotary installation compared to a monotonic push and thus the width of the plastic deformation zone increases as AR decreases. The value of L_{pv} ($3D_h$) is based upon the region of shearing observed by Lu *et al.* (2004). The value of $4D_h$ for L_{pr} was chosen based upon the results of 1g tests conducted by Garcia - Galindo *et al.* (2018) in which surface mechanisms were observed at up to $4D_c$ from the centre of a rotary installed straight shafted pile during 1g testing.

In this study two methods of installation were considered. The first was a screw pile installed at a constant AR (although AR varies between tests) and the second is a screw pile installed at a constant vertical compressive force equal to its own “self-weight”. When installing the screw pile at a constant AR in DEM, displacement control was used. The vertical and angular velocities of the pile were calculated using Equations 6 - 9 and applied to the pile sufficiently slowly to ensure that a quasi-static regime was maintained. When installing the pile under “self-weight” (or fixed crowd) installation in DEM, a force control servo was applied. To do this the angular velocity of the pile was fixed for the entirety of the simulation and the vertical velocity was controlled through a feedback loop. The feedback loop calculated the sum of the vertical component of the contact forces between

the screw pile and the soil at a given moment in time and compared it to the prescribed value. If the vertical force was below that which was required, the vertical velocity was increased and if the vertical force was higher, the vertical velocity for the next step was decreased. The maximum vertical velocity was capped near to the surface ($z < 0.5\text{m}$ only), to produce an $AR = 1$, to ensure a quasi-static regime was maintained throughout the installation. The self-weight of the pile considered in this study was 640kN. To obtain the axial capacity of the installed piles constant rate of penetration (CRP) (Brown 2012) tests were conducted, and the installed piles were displaced vertically by $0.5 D_h$ at a constant velocity of 0.1m/s and the vertical force acting on the pile was continuously recorded using inbuilt commands within the software. To achieve this, the command loops through all of the contacts between the particles and the pile and sums the vertical force component of each contact force.

All simulations undertaken in this study were conducted using an Intel Xeon E5-2639v3 PC with 32GB of RAM. The computational time required for fixed AR installation and axial testing ranged between 22 hours and 26 hours. The computational time of the self-weight installation ranged between 50 hours and 70 hours, reflecting the influence of the servo control. More information on the times for soil bed formation are shown in Table 2.

3 Results and discussion

3.1 Effect of AR on installation resistance

The results from the installation of the pile in all of the soil densities can be seen in Figure 3. This figure highlights the large vertical crowd forces (15MN in dense sand) and torques (5MNm in dense sand) that may be encountered when trying to install a screw pile designed for offshore application where pitch-matched guidance is followed ($AR = 1$). It can be seen that varying the advancement ratio has a significant effect on the vertical compressive force during installation with a 96% reduction in force when moving from pitch matched installation to self-weight installation. During

self-weight installation the AR progressively reduced from 1.1 at 2m depth to 0.5 at the final depth (Figure 4).

AR has a reduced effect on the installation torque with a pronounced effect only at the extremes of under-fighting and self-weight installation, which shows an increase and reduction of torque requirement, respectively (Figure 3b, 3d and 3f). This is in agreement with the *DEM* study of Shi *et al.* (2019) as well as the 1g physical modelling studies of Shi *et al.* (2018) and Kenny *et al.* (2003), who all noted a large decrease in compressive installation force and a smaller decrease in installation torque when installing at lower AR values. Thus, it would seem there is potential for reducing vertical load (or crowd) requirements during installation by reducing the AR to below the recommended “perfect” or pitch matched installation. However, the potential effect of the advancement ratio on the in-service performance must be considered.

The large reductions in installation force that are seen when over-fighting ($AR < 1$), in addition to the anecdotal evidence that screw piles are able to screw themselves in, suggests that most if not all onshore screw piles are actually over fought to some degree when installed in the field.

3.2 Effect of AR on in-service compressive and tensile capacity

The effect of the variation in AR on the in-service post installation capacity is shown in Figure 5 for all soil densities. The markers shown in Figure 5 are for identification purposes only and do not represent the data points. The data is continuously recorded during the axial capacity test and is represented by the lines of the force displacement curve. If the capacity is defined in the conventional manner as recommended by SPERW (Institute of Civil Engineers 2017) and AC358 (International Code Council 2017) as the resistance at a pile displacement equivalent to $y/D_h = 0.1$ (where y is the vertical displacement during axial loading) it can be seen that under fighting ($AR = 1.2$) results in the greatest compressive capacity in all soil densities (8MN in loose, 24MN in medium dense and 33MN in dense) (Figure 5a, 5c and 5e) but also has the highest installation force requirements (8MN in loose, 14MN in medium dense and 20MN in dense) (Figure 3a, 3c and 3e).

Low AR (over flying $AR = 0.5$) has the worst performance in compression but the self-weight installation is slightly better than this and is about 21% lower than the pitch matched installation at a pile displacement of $0.1D_h$ in the medium dense and dense soil beds. Low displacement stiffness (e.g. $y/D_h < 0.02$) appears to be unaffected by AR . At much greater displacements ($y/D_h > 0.3$) the effect of the installation approach on compressive resistance is also less noticeable although the low AR installation still results in reduced resistance. From Figure 5b, 5d and 5f the opposite is generally true when considering tensile performance. In these cases, a low AR or self-weight installation results in capacity and stiffness that is 43% greater than pitch matched installation at a displacement of $0.1D_h$ in the medium dense and dense soils, with the loose soil bed showing an increase of up to 120% compared to pitch-matched installation.

In contrast to the compressive resistance tests the tensile resistance shows a significant drop in low displacement stiffness with increasing AR . These effects are not overcome until significant uplift displacements are reached ($y/D_h = 0.4$). Thus, over-flying ($AR < 1$) can significantly reduce installation requirements and has a beneficial effect on tensile performance at the expense of some compressive capacity. This seems to be at odds with the assumptions of BS 8004:2015 and suggests over-flying may be beneficial for offshore screw and tension only anchor designs. These results show that a low AR can reduce the vertical compressive force required for installation, as also shown by Shi *et al* (2019), which assists in installation plant design where there is still a considerable need for torque input, without compromising tensile capacity performance, which is controlling in the design of offshore screw piles (Davidson *et al.* 2020).

3.3 Summary of effects of AR on installation resistance and in-service capacity

A summary of the effect of AR across all densities is shown in Figure 6. The torque and force quantities have been normalised by the values for pitch-matched installation ($AR = 1$). Figure 6a and 6b show the installation force and torque while Figures 6c and 6d show the compressive and tensile capacity, defined at $y/D_h = 0.1$. The slope of the fitted lines shows the strength of the effect of AR on each quantity. By reducing AR , there is a significant reduction in compressive installation force (up to

61%), a reduction in installation torque (up to 35%) and compressive capacity (up to 39%), but a strong increase in tensile capacity (up to 120% increase in loose and 60% in other densities) when compared to the pitch-matched installation. These trends are generally consistent across all relative densities. The only strong outliers in terms of density are the normalised tensile capacities for $AR < 1$ in loose soil, which are much greater than for the other two soil densities.

Figure 6c and 6d also indicate that installing screw piles between an AR of 0.8 and 1.2 does not equate to a reduction in “soil disturbance”, as suggested by BS 8004: 2015, due to the significantly lower tensile capacity at these AR values. However, the normalised axial capacities show that “soil disturbance” is a relative term highly dependent upon whether the installed pile is to be loaded in tension or compression, as indicated by the trends discussed above (Figure 6c and 6d). The advancement ratio calculated using Equation 2 ($AR = 0.72$) proposed by Viggiani (1989), for CFA piles, appears to strike a balance between compressive and tensile capacity. At this AR there is a limited decrease in compressive capacity (10%) and a substantial increase in tensile capacity (27% in medium dense and dense sand and 114% in loose sand), while having a beneficial effect on the installation requirements when compared to the pitch matched case. This further undermines the guidance from BS8004 and shows that other approaches also do not agree with the recommendations of BS8004. Highlighting that there is further scope for optimisation of advancement ratio depending on the required use of the screw pile.

3.4 Effect of AR on soil failure mechanism during uplift

To determine the cause of this large increase in tensile capacity in the loose soil bed, the average particle displacement (U) during the tensile capacity test was investigated for the screw piles installed at $AR=0.5$ and $AR = 1$. Figure 7 shows that a different mechanism occurs when the pile is over-flighted during installation. The over-flighted screw pile ($AR = 0.5$, Figure 7a) has a larger influence zone during the tensile uplift test and is developing a conical failure wedge, while the pitch-matched pile ($AR = 1$ Figure 7b) results in a localised flow around mechanism, around the screw pile helix, producing a lower tensile resistance.

387 This difference in mechanism during uplift between $AR = 1$ and $AR = 0.5$ in the loose soil is produced
388 by the difference in the local soil density post-installation. By extracting the radial and vertical
389 position and volume of each particle in the soil bed pre and post-installation it is possible to
390 determine the change in relative density caused by the installation of the screw pile. To calculate the
391 relative density at a given point, the soil bed is partitioned into several 3D annular cylinders (coaxial
392 cylinders) delimited by radial and vertical position as undertaken by Ciantia et al. (2019). The
393 dimensions of each annulus were determined by the particle scaling used within the region it lies,
394 such that smaller annuli are present in the core of the soil bed and larger annuli are required at the
395 boundary. The size of the annuli were chosen to give an optimal balance between resolution, which
396 decreases with increasing annulus size, and achieving a statistically representative volume which
397 requires a minimum of 60 particles (Ciantia et al. 2019). The volume of the annulus and the particles
398 residing within it are known quantities and from this a voids ratio and therefore a relative density
399 can be calculated. Comparing the relative density of each annulus pre and post installation the
400 change in relative density can be determined and assigned accordingly. The value for each annulus is
401 then plotted according to its vertical and radial position to create a contour plot, as shown in Figure
402 7c and 7d, which represent an axisymmetric averaging of the change in relative density of the soil
403 body projected on a 2D plane. Figure 7c and 7d show the change in relative density as a result of the
404 installation of the screw pile into the loose soil bed at $AR = 0.5$ and 1.0 . From Figure 7c and 7d it can
405 be seen that the installation of the pitch-matched screw pile has decreased the relative density of
406 the soil surrounding the shaft by approximately 25%, whereas for the over-flighted screw pile (AR
407 $= 0.5$) there is an increase in relative density in the same region of 10%. The denser soil surrounding
408 the over-flighted screw pile increases the uplift resistance as the failure mechanism must now
409 propagate through denser soil. The increase in density also resulted in a change in the mechanism
410 from a flow around, typically seen in loose soil (Figure 7b), to a wedge type failure (figure 7a), giving
411 the over flighted screw pile a drastic increase in uplift resistance as shown in Figure 3b.

412 In the medium dense soil and the dense soil beds a similar effect was seen, where the over-flighted
413 screw pile installation ($AR < 1$) resulted in denser soil surrounding the pile post installation compared
414 to the pitch-matched or under-flighted installation. Unlike the loose case the relative density of the
415 over-flighted installation in the dense and medium dense soil did not increase with respect to the
416 initial state. The failure mechanism for all AR values in the denser soil beds resulted in a wedge type
417 failure, with the increase in tensile capacity attributed to the increase in the dilation angle of the
418 denser soil surrounding the pile post-installation. Figure 8 shows the zone of influence of the screw
419 pile during an uplift capacity test in the Dense soil bed ($D_r = 83\%$). It can be seen that the over
420 flighted screw pile had a larger zone of influence than the pitch-matched one as also seen in the
421 loose soil bed in Figure 7, in addition to an increased zone of intense displacement seen above and
422 around the helix in Figure 8 (denoted by the zones tending towards white shading). Using the
423 relative density index proposed by Bolton (1986), the dilation angle of soil at various depths were
424 calculated and integrated to create an approximated failure surface. The screw pile shown in figure 8
425 is shown in it's final position at the end of the uplift phase. Calculation of the dilation angle and the
426 derived failure surface is shown based upon the original position of the screw pile at some lower
427 depth with the failure plane assumed to propagate from the outer edge of the helix plates. It is
428 noted that the dilation angle shown here is not an input required for the DEM simulation but has
429 been added to show the similarity of the DEM observed failure mechanisms (zones tending towards
430 white shading) to other studies where it has previously been proposed that the shallow failure
431 wedge propagates upwards inclined at the dilation angle (Giampa et al. 2017; Cerfontaine et al 2019;
432 Liu et al 2012). If the in-situ pre-installation relative density and mean effective stress (p') are used, a
433 linear failure surface akin to that proposed by Giampa *et al.* (2017) is created (shown on the left of
434 figures 8a and 8b). This failure surface is simplistic in nature and lies outside the central zone of
435 intense displacement, most notably when close to the helix of the pile. When using the post
436 installation relative density and p' exported from the DEM simulations, the approximated failure
437 surface fits the outline of the zone of intense displacement closely. Particles which lie outside of this

failure surface show very little displacement (denoted by their dark grey shading). The failure surface is non-linear, starting near vertical at the helix of the pile before expanding out to form a cone as it propagates towards the surface, similar in shape to the wedge type failure observed for shallow plate anchors by Liu *et al.* (2012) using digital image correlation on model scale experiments. This non-linearity of the failure surface is due to the suppression of the soil dilatancy angle in the high stress region close to the base of the screw pile, which reduces as it tends towards the surface. The higher relative density of the soil surrounding the pile in the AR = 0.5 installation (Figure 8a), results in a larger dilation angle, which manifests as a 0.5m increase in the radial extent of the wedge at the soil surface. The increase in tensile capacity in Figure 5f in the denser soils is attributed to this increase in the dilation angle post installation.

3.5 Effect of AR on torque correlation factor

Exploring the results in terms of a torque correlation factor as per Equation 3 where K_t denotes tension and K_c denotes compression it can be seen that the values of K_c and K_t were not the same as proposed by Perko (2009) and varied quite significantly K_c from = 5.3-6.3 and K_t from 0.7 to 2.3 (in dense soil) for the large diameter plugged piles simulated here (Figures 9a and 9b). This in line with the findings of Davidson et al (2020) who showed that K_c and K_t varied significantly in the results of centrifuge testing of screw piles designed for offshore use ($H/D_h = 4.6 - 7.4$). Typical results from centrifuge testing are shown in Figure 9 to aid comparison and to act as further evidence of previous validation of the DEM approach used. Therefore, it would appear that it is not appropriate to assume the same torque correlation factor for both tension and compression loading for this geometry of pile and depth effect or H/D_h should be considered. Comparing the effect of advancement ratio on K_c & K_t shows a marked difference where AR significantly effects K_t but there is little effect on K_c for a given density. This is likely to be as a result of the very different mechanisms found during tensile and compressive loading. In compression the pile has a large localised end-bearing component which will be defined by the diameter of the helix with a relatively small contribution from the shaft. In tension a wedge type failure was produced (Figure 8), with the angle

of the wedge equal to that of the dilation angle of the soil the wedge is propagating through (Giampa *et al.* 2017; Cerfontaine *et al.* 2019) resulting in the capacity being primarily effected by the relative embedment depth, the soil relative density and the mean effective stress post installation, and by the diameter of the helix ($H/D_h = 7$ for this study). Therefore, the much higher magnitude of K_c relative to K_t and the obvious difference in the values.

3.6 Effect of AR on residual stresses around pile

Figure 9a also shows that the K_t factor is density dependent with medium dense sand showing the highest values and loose sand giving the lowest. This is due to the difference in relative density of the soil that is encountered during the installation and the post installation tensile capacity tests. During installation, the torque correlates directly with the applied vertical force due to the increased vertical stress component of interface shearing resistance on the base and helix surfaces i.e. helix torque is controlled by an interface shearing mechanism. The base of the screw pile and therefore the helix is continuously penetrating into virgin soil during the installation and therefore the installation torque is controlled by the initial soil conditions. In contrast to this, the tensile capacity is governed by the soil state above the helix post-installation as the mechanism must propagate through this. The percentage change in relative density, surrounding the helix and pile shaft, is lower in the medium dense sand (18% reduction for $AR = 1$) than it is dense sand (23% reduction for $AR = 1$). This difference in relative density change resulted in the medium dense soil showing a larger K_t factor as the relative density of the soil controlling the installation torque and tensile capacity are similar in value. Previous studies such as Jeffrey *et al.* (2016) have shown this effect through the use of cone penetration tests conducted at various distances from installed cast in-situ screw piles post-installation.

Varying AR resulted in the variation of the required vertical compressive force applied to the pile head and subsequently the base of the pile, during installation. The large compressive forces required during installation at higher AR values resulted in large residual stresses (Cooke 1979) (or a locked in stress regime) below the pile as shown in Figure 10 which increased with increasing AR as

suggested by Viggiani (1989) for CFA installation and previously observed through DEM by Shi *et al* (2019). The locked in stress below the helix during installation for $AR > 1.0$, preloaded the soil below the helical plate resulting in a post installation compressive stiffness which was far greater than that of the over-flighted case (Figure 5a,5c and 5e). For the under-flighted and pitch-matched installations a region of very low stress, one helix diameter in height was seen above the helix. This region of low stress resulted in the shaft of the screw pile providing very limited resistance during compressive loading, as suggested by Tappenden and Sego (2007), Mohajerani *et al.* (2014); and Davidson *et al.* (2020). In the over-flighted cases, the low stress region above the helix is no longer present and therefore the shaft would provide additional compressive resistance, although it should be noted that the increase in shaft resistance did not counteract the decrease in stiffness attributed to the reduction of locked in or residual stress below the helix.

When assessing the effects of the post installation residual stress field on the tensile capacity, the reverse was true. The over flighted piles had a larger stiffness in tension and due to the large vertical stresses observed above the helix and an increase in capacity due to the increase in dilation angle (Figure 8), compared to the region of low stress found in the pitch-matched and under-flighted installations. As a shallow mechanism (i.e. a wedge) was formed propagating from the helix tip to the surface, the shaft had very little influence on the tensile resistance for the geometry presented in this study (Cerfontaine *et al.* 2020).

3.7 Effect of AR on soil movement during installation

To assess how the post installation stress field and the changes in relative density of the soil surrounding the pile occurred, the displacement of soil particles during the different installation processes was investigated for a pitch-matched and over-flighted ($AR = 0.5$) pile. When the pile is pitch-matched (or under-flighted $AR = 1-1.2$), particles were primarily displaced downwards and radially (Figure 11), causing a flow-around mechanism akin to a bearing capacity failure below the helix of the screw pile. The downwards movement preloaded the soil below the helix locking in the high levels of vertical stress (Figure 10) increasing compressive stiffness and capacity.

The displacement of the particles during the installation can also be used to demonstrate how a region of low relative density soil was formed around the pile shaft for pitch-matched installation. Pitch-matched installation encouraged soil to move away from the shaft of the pile and around the helix, momentarily forming a small cavity behind the helix which then collapsed and filled with soil that was looser than the initial conditions (Figure 7d). When the screw pile was over-flighted during installation ($AR < 1$) the movement of the helix encouraged soil to move through the helix rather than radially around the helix (Figure 11), similar in mechanism to that of an Archimedean screw. This phenomenon has previously been observed by Hird *et al.* (2008, 2011) when over and under-flighting a CFA tool using transparent soil analogues and by Shi *et al.* (2019) when installing a screw drill pile at various advancement ratios. The observations of Hird *et al.* (2008,2011) show that when under-flighting, particles displace downwards and radially away from the base of the CFA, in contrast to the purely upward movement of the particles when the CFA tool was over-flighted during the installation process. The DEM study of Shi *et al.* (2019) observed particles moving predominantly in the downwards direction when under-flighting and upwards when over flying, which is consistent with the findings of this study.

The upward movement reduced the volume of soil that was displaced below and around the helix and in turn produced a denser soil surrounding the shaft and helix and a reduced vertical stress field below the screw pile helix post-installation. This also removed the low stress region above the helix observed for pitch-matched installation. The upward movement of the soil also appeared to reduce the loosening of the soil, so that it is closer to its initial conditions (Figure 7c) than in the pitch matched case (Figure 7d). This in turn gave the soil a higher tensile capacity and tensile stiffness (Figure 6d).

3.8 Effect of AR on dimensionless torque factors

The effects of the helix on the pile response suggest that it would be more appropriate to correlate the K_c value with helix diameter rather than shaft diameter as proposed by Perko (2009) which is in line with that proposed by Byrne & Houlsby (2015) (Figure 12b). However, it should be noted that

incorporating the helix diameter into K_c does not remove the large density effects that are seen in this study. Although the dense and medium dense sand beds (which would be typically seen in the offshore environment) produce K_c^* values within the range of those proposed by Byrne & Houlsby (2015), the loose soil bed produced K_c^* below the proposed values. As previously discussed, in tension the mechanism for uplift resistance was very different from that in compression because an uplifting wedge was formed, propagating from the edge of the helix to the soil surface as per Cerfontaine *et al.* (2019) for the relatively short pile used in this study ($H/D_h=7$) (Figure 13), again suggesting correlation with D_h rather than D_c (Figure 12a). However, the installation torque in the main is dependent on the total area of the pile elements including the shaft component which may be of large diameter in offshore applications. As the values for K_t^* proposed by Byrne & Houlsby (2015) are formulated on the assumption of a deep tensile mechanism, they are not appropriate for screw piles at $H/D_h < 7$ where the conical uplift mechanism has been shown to form, both numerically in this study (Figure 8 and 13b) and observed in centrifuge tests by Davidson *et al.* (2020). This highlights the need to consider H/D_h appropriately in any analysis or prediction.

3.9 Effect of pile length of torque factors

Although all of the screw piles used in this study were installed to shallow relative embedment depths (due to the large relative diameter of the helices required for offshore use), it is prudent to note that most onshore screw piles will be installed to deeper relative embedment depths ($H/D_h > 10$) due to their small helix diameters. Therefore, it is assumed that the axial capacity tests used to formulate Equation 3 have been based upon “deep” pile tests where a deep mechanism forms when tested under tension (Figure 13d). For a screw pile, this would result in a reverse bearing capacity or flow around mechanism, with an axial tensile capacity similar to that of an axial compression test.

To test if this is the origin of differences between onshore observations of unique K values and equal values in tension and compression, four simulations of the same pile configuration (shown in Figure 1b) were installed to a $H/D_h = 11$ (i.e. pile core and helix diameters were kept as previous but the depth of installation was increased to 18.7 m) and axially tested in the dense soil bed after

installation at AR values ranging between 0.5 and 1.2. Figure 14a and 14b show the K_t and K_c values for all simulations conducted within the dense soil bed, the axial capacity for all results are considered at the same displacement level. From Figure 14 it can be seen that when the screw pile is installed to a deeper relative embedment, the torque-capacity correlation factor for compression and tension are similar in magnitude ($K_t = 0.45$ $K_c = 1.11$) which explains the suggestion of similar values of K_t and K_c by Perko (2009). Although AR still influences the K_t value, it is much less pronounced for a deep mechanism compared to those of a shallow mechanism, as previously seen when assessing K_c values. As the relative embedment depth increases ($H/D_h > 11$) it may be possible that the difference between K_t and K_c becomes ever smaller, as the installation torque would increase at a higher rate than that of the axial capacity and thus explaining previous assumptions of similar values of K in compression and tension.

The above discussion highlights that for the single pile geometry investigated here that K_c is relatively insensitive to AR whereas K_t is significantly affected by both AR and installation depth. This suggests that torque correlation factors cannot be considered unique or a single value for a screw pile geometry and depth as they can be significantly influenced by how the pile is installed i.e. under or over-flighted. This is not something that is conventionally measured in commercial screw pile installations and suggest that rotation and advancement rate measurements along with direct torque measurement should be automated and become routinely determined in practice. It is also notable that the value of K_t and K_c are not independent of soil density as current approaches would suggest, with loose soils giving much lower values of K compared to medium and dense sand, where the values are relatively similar (Figure 9). Thus, using analytically derived pile capacity to determine installation requirements via K maybe inaccurate and using torque during installation to verify the adequacy of pile installation maybe unsafe. This is especially so where larger shallow or deep piles of different geometry may be required for offshore deployment in the renewable energy sector.

4 Conclusion

In this paper the effects of advancement ratio on the axial in service performance of a single screw pile geometry has been investigated using the Discrete Element Method in sand of different relative densities. The screw pile geometry is that which has been previously designed and model tested for offshore renewable energy applications as a replacement for driven piles. The investigation has shown that by over-fighting ($AR < 1$) a screw pile during installation, compared to installation at pitch-matched ($AR = 1.0$) it is possible to reduce the installation force required significantly (up to 96%) and it is possible to install a screw pile under its own self-weight. The installation torque is less effected by AR , but it is possible to reduce the required installation torque (up to 35%) by over-fighting. The results of the in-service axial capacity tests have shown that although over-fighting reduces the compressive capacity (up to 39%) of a screw pile, it is also able to significantly increase the capacity and stiffness of the screw pile when loaded in tension (up to 120% in loose soil and 60% in other densities). Using interparticle contact forces and particle displacements exported from the DEM simulations, it has been shown that the AR chosen during installation has a significant effect on the in-service behaviour of the screw pile due to the residual stress field surrounding the pile post-installation.

The results of the investigation were then used to assess the applicability of the empirical torque capacity correlation factors K_t and K_c on larger diameter screw piles for offshore renewable energy deployment. The assumption that a screw pile has a single K value solely based upon its geometry has been shown to be inappropriate for these larger screw piles. The results have shown that several different factors contribute to both the installation torque and the ultimate capacity which have previously seen little attention such as the advancement ratio, soil relative density and the relative embedment depth. This implies that using analytically derived pile capacity to determine installation requirements maybe inaccurate and using torque during installation to verify the adequacy of a single helix pile installation maybe unsafe especially where different or larger pile geometries are adopted.

618

619 **5 Acknowledgements**

620 This research is a part of an EPSRC NPIF funded studentship with Roger Bullivant Limited (Grant no.

621 EP/R512473/1). The 3rd author is supported by the European Union's Horizon 2020 research and

622 innovation programme under the Marie Skłodowska-Curie grant (Agreement No 753156). The

623 authors would also like to acknowledge the support of EPSRC: Supergen Wind Hub: Grand

624 Challenges Project: Screw piles for wind energy foundations (Grant no. EP/N006054/1) for the

625 impetus for this study.

626

Draft

6 References

- Al-Baghdadi, T. 2017 *Screw piles as offshore foundations : Numerical and physical modelling*. Ph.D thesis, School of Science and Engineering, University of Dundee, Dundee, U.K.
- Al-Defae, A. H., Caucis, K. and Knappett, J. A. 2013 'Aftershocks and the whole-life seismic performance of granular slopes', *Géotechnique*, 63(14), pp. 1230–1244. doi: 10.1680/geot.12.P.149.
- Arroyo, M., Butlanska, J., Gens, A., Calvetti, F. and Jamiolkowski, M. 2011 'Cone penetration tests in a virtual chamber', *Géotechnique*, 61(6), pp. 525–531. doi: 10.1680/geot.9.P.067.
- Bolton, M. D. 1986 'The strength and dilatancy of sands', *Geotechnique*, 36(1), pp. 65–78.
- Bolton, M. D., Gui, M. W., Garnier, J., Corte, J. F., Bagge, G., Laue, J. L. and Renzil, R. 1999 'Centrifuge cone penetration tests in sand', *Géotechnique*, 49(4), pp. 543–552. doi: 10.1680/geot.1999.49.4.543.
- Bradshaw, A., Zuelke, R., Hilderbrandt, L., Robertson, T. and Mandujano, R. 2019 'Physical Modelling of A Helical Pile Installed in Sand Under Constant Crowd', in Davidson, C., Brown, M. J., Knappett, J. A., Brennan, A. J., Augarde, C. E., Coombs, W. M., Wang, L., Richards, D., White, D. J., and Blake, A. (eds) *ISSPEA*. Dundee, UK: University of Dundee, pp. 109–115. doi: 10.20933/100001123.
- British Standards Institute 2015 *BS8004: Code of practice for foundations*. London, UK.
- Brown, M.J. 2012 'Pile capacity testing', in Burland, J., Chapman, T., Skinner, H., and Brown, M.J. (eds) *ICE manual of Geotechnical Engineering*. 1st edn. London United Kingdom: ICE Publishing Limited, pp. 1451–1469. doi: 10.1680/moge.57098.1451.
- Butlanska, J., Arroyo, M., Gens, A. and O'Sullivan, C. 2014 'Multiscale analysis of CPT in a virtual calibration chamber', *Canadian Geotechnical Journal*, 26(1), pp. 80–86. doi: 10.1139/cgj-2012-0476.
- Byrne, B. W. and Houlsby, G. T. 2015 'Helical piles: an innovative foundation design option for offshore wind turbines', *Philosophical Transactions of the Royal Society A: Mathematical, Physical & Engineering Sciences*, 373, pp. 1–11. doi: 10.1098/rsta.2014.0081.
- Cerfontaine, B., Brown, M. J., Knappett, J. A. and Davidson, C. 2019 'Finite Element Modelling of the Uplift Behaviour of Screw Piles in Sand', in Davidson, C., Brown, M. J., Knappett, J. A., Brennan, A. J., Augarde, C. E., Coombs, W. M., Wang, L., Richards, D., White, D. J., and Blake, A. (eds) *ISSPEA*. Dundee, UK: University of Dundee, pp. 69–75. doi: 10.20933/100001123.

Cerfontaine, B., Knappett, J. A., Davidson, C., Brown, M. J., Brennan, A. J., Al-Baghdadi, T., Augarde, C. E., Coombs, W., Wang, L., Blake, A., Richards, D. and Ball, Jonathan, D. 2020 'A Finite Element approach for determining the full load-displacement relationship of axially-loaded screw anchors, incorporating installation effects', *Canadian Geotechnical Journal*. Published online 30/06/20. doi: doi.org/10.1139/cgj-2019-0548.

Ciantia, M. O., Arroyo, M., Butlanska, J. and Gens, A. 2016 'DEM modelling of cone penetration tests in a double-porosity crushable granular material', *Computers and Geotechnics*, 73, pp. 109–127. doi: 10.1016/j.compgeo.2015.12.001.

Ciantia, M. O., Boschi, K., Shire, T. and Emam, S. 2018 'Numerical techniques for fast generation of large discrete-element models', *Proceedings of the Institution of Civil Engineers - Engineering and Computational Mechanics*, 171(4), pp. 147–161. doi: 10.1680/jencm.18.00025.

Ciantia, M. O., O'Sullivan, C. and Jardine, R. 2019 'Pile penetration in crushable soils: Insights from micromechanical modelling', in *XVII ECSMGE-2019*. Reykjavik, Iceland, pp. 298–317. doi: doi: 10.32075/17ECSMGE-2019-1111.

Cooke, R. W. 1979 'Influence of Residual Installation Forces on the Stress Transfer and Settlement Underworking Loads of Jacked and Bored Piles in Cohesive Soils', in Lundgren, R. (ed.) *Behavior of Deep Foundations*. West Conshohocken, PA: ASTM International, pp. 231–249. doi: 10.1520/STP33731S.

da Cruz, F., Emam, S., Prochnow, M., Roux, J.-N. and Chevoir, F. 2005 'Rheophysics of dense granular materials: Discrete simulation of plane shear flows', *Physical Review E*. American Physical Society, 72(2), pp. 1–17. doi: 10.1103/PhysRevE.72.021309.

Das, B. M. and Shukla, S. . 2013 *Earth Anchors*. USA: J. Ross Publishing.

Davidson, C., Al-Baghdadi, T., Brown, M. J., Brennan, A., Knappett, J., Augarde, C. E., Coombs, W., Wang, L., Richards, D., Blake, A. and Ball, J. 2018 'A modified CPT based installation torque prediction for large screw piles in sand', in Hicks, M. A., Federico, P., and Peuchen, J. (eds) *Cone Penetration Testing*. Delft, Netherlands: CRC Press, pp. 255–261. doi: https://doi.org/10.1201/9780429505980.

Davidson, C., Brown, M. J., Brennan, A. J., Knappett, J. A., Cerfontaine, B. and Sharif, Y. U. 2019 'Physical modelling of screw piles for offshore wind energy', in Davidson, Craig ;, Brown, Michael J., Knappett, Jonathan Adam, Brennan, Andrew J., Augarde, C. E., Coombs, W. M., Wang, L., Richards, D., White, D. J., and Blake, A. (eds) *ISSPEA*. Dundee, United Kingdom: University of Dundee, pp. 31–38. doi: 10.20933/100001123.

Davidson, C., Brown, M.J., Cerfontaine, B., Knappett, J.A., Brennan, A.J., Al-Baghdadi, T., Augarde, C., Coombs, W., Wang, L., Blake, A., Richards, D.J. & Ball, J.D. Feasibility of screw piles for offshore jacket structures. *Geotechnique*. ISSN 0016-85052. Published online 23/09/20. DOI: 10.1680/jgeot.18.P.311.

Duan, N., Cheng, Y. P. and Liu, J. W. 2018 'DEM analysis of pile installation effect: comparing a bored and a driven pile', *Granular Matter*. Springer Berlin Heidelberg, 20(3), pp. 1–16. doi: 10.1007/s10035-018-0805-2.

Garcia - Galindo, P., Davidson, C. ; and Brown, M. J. 2018 'Installation Behavior of Open Ended and Closed Ended Piles with Torque Application', in *1st International conference of Press-in Engineering*. Kochi, Japan, pp. 379–386.

Garnier J, Gaudin, C., Springman, S. M., Culligan P, Goodings, D., Konig, D., Kutter, B., Phillips, R., Randolph, M. and Thorel, L. 2007 'Catalogue of scaling laws and similitude questions in geotechnical centrifuge modelling', *International Journal of Physical Modelling in Geotechnics*, 7(3), pp. 1–23.

Gavin, K., Doherty, P. and Spagnoli, G. 2013 'Prediction of the installation torque resistance of large diameter helical piles in dense sand.', in Lutenegeger, A. J. (ed.) *1st Int. Geotechnical Symp. of Helical Foundations*. Amherst, USA, pp. 131–140.

Giampa, J., Bradshaw, A. and Schneider, J. 2017 'Influence of Dilation Angle on Drained Shallow Circular Anchor Uplift Capacity', *International Journal of Geomechanics*, 17(2), pp. 1–11. doi: <https://dx.doi.org/10.1061/>.

Hird, C. C., Ni, Q. and Guymer, I. 2008 'Physical Modelling of Displacements Around Continuous Flight Auger in Clay', in Brown, M. J., Bransby, M. F., Brennan, A. J., and Knappett, J. A. (eds) *Proceedings of the Second International British Geotechnical Association Conference on Foundations*. Dundee, UK: Bre Press, pp. 566–574.

Hird, C. C., Ni, Q. and Guymer, I. 2011 'Physical modelling of deformations around piling augers in clay', *Geotechnique*, 61(11), pp. 993–999. doi: 10.1680/geot.9.T.028.

Houlsby, G. T. 2016 'Interactions in offshore foundation design', *Géotechnique*, 66(10), pp. 791–825. doi: 10.1680/jgeot.15.RL.001.

Hoyt, R. . and Clemence, S. P. 1989 'Uplift capacity of helical anchors in soil', in *Proceedings of the 12th International conference on Soil Mechanics and Foundations*. Rio de Janeiro, pp. 1019–1022.

Institute of Civil Engineers 2007 *ICE Specification for Piling and Embedded Retaining Walls*, ICE Specification for Piling and Embedded Retaining Walls. ICE Publishing. doi: 10.1680/icesperw.61576.

International Code Council 2017 *AC308 Helical Pile Systems and Devices*. Available at: <https://iccs.org/acceptance-criteria/ac308-2/>.

Itasca Consulting Group, I. 2016 'PFC 5.0'. Minneapolis: Itasca Consulting Group, Inc.

Janda, A. and Ooi, J. Y. 2016 'DEM modelling of cone penetration and unconfined compression in cohesive solids', *Powder Technology*, 293(5), pp. 60–68. doi: <https://doi.org/10.1016/j.powtec.2015.05.034>.

Jeffrey, J. R., Brown, M. J., Knappett, J. A., Ball, J. D. and Caucis, K. 2016 'CHD pile performance: part I – physical modelling', *Proceedings of the Institution of Civil Engineers - Geotechnical Engineering*, 169(5), pp. 421–435. doi: 10.1680/jgeen.15.00131.

Kenny, M. ., Guasti, S. and Zsak, P. 2003 'Continuous flight auger boring in sandy soils', in *Proceedings BGA International Conference on Foundations*. Dundee, UK: Thomas Telford Ltd, pp. 433–441.

Klinkvort, R. T., Springman, S. M. and Hededal, O. 2013 'Scaling issues in centrifuge modelling of monopiles', *International Journal of Physical Modelling in Geotechnics*, 13(2), pp. 38–49. doi: 10.1680/ijpmg.12.00010.

Knappett, J. A., Brown, M. J., Brennan, A. J. and Hamilton, L. 2014 'Optimising the compressive behaviour of screw piles in sand for marine renewable energy applications', in *11th International Conference on Piling and Deep Foundations*. Stockholm, Sweden: Deep Foundations Institute, p. Article #1904.

Lauder, K. 2010 *The performance of pipeline ploughs*. Ph.D thesis, School of Science and Engineering University of Dundee, Dundee. U.K.

Lauder, K. D., Brown, M. J., Bransby, M. F. and Boyes, S. 2013 'The influence of incorporating a forecutter on the performance of offshore pipeline ploughs', *Applied Ocean Research*, 39, pp. 121–130. doi: 10.1016/j.apor.2012.11.001.

Li, Z., Haigh, S. K. and Bolton, M. D. 2010 'Centrifuge modelling of mono-pile under cyclic lateral loads', *Physical Modelling in Geotechnics - Proceedings of the 7th International Conference on Physical Modelling in Geotechnics 2010, ICPMG 2010*, 2, pp. 965–970. doi: 10.1201/b10554-159.

Liu, J., Liu, M. and Zhu, Z. 2012 'Sand Deformation around an Uplift Plate Anchor', *Journal of*

Geotechnical and Geoenvironmental Engineering, 138(6), pp. 728–737. doi: 10.1061/(ASCE)GT.1943-5606.0000633.

Lu, Q., Randolph, M. F., Hu, Y. and Bugarski, I. . 2004 'A numerical study of cone penetration in clay', *Géotechnique*, 54(4), pp. 257–267. doi: 10.1680/geot.2004.54.4.257.

Lutenegger, A. J. 2013 'Factors Affecting Installation Torque and Torque-To-Capacity Correlations for Screw-Piles and Helical Anchors', in *Proceedings of the 1st International Geotechnical Symposium on Helical Foundations*, pp. 211–224.

Lutenegger, A. J. 2019 'Screw Piles and Helical Anchors- What we Know and What we Don't Know: An Academic Perspective - 2019', in Davidson, C. ;, Brown, M. J., Knappett, J. A., Brennan, A. J., Augarde, C. E., Coombs, W. M., Wang, L., Richards, D., White, D. J., and Blake, A. (eds) *ISSPEA*. Dundee, UK: University of Dundee, pp. 15–28. doi: 10.20933\100001123.

Lutenegger, A. J. and Tsuha, C. D. H. C. 2015 'Evaluating installation disturbance from helical piles and anchors using compression and tension tests', in *Proceedings of the 15th Pan-American Conference on Soil Mechanics and Geotechnical Engineering*. Buenos Aires, Argentina, pp. 373–381. doi: 10.3233/978-1-61499-603-3-373.

Martinez, A., DeJong, J., Jaeger, R. and Khosravi, A. 2020 'Evaluation of the self-penetration potential of a bio-inspired site characterisation probe by cavity expansion analysis', *Canadian Geotechnical Journal*, 57(5), pp. 706–716. doi: <https://doi.org/10.1139/cgj-2018-0864>.

McDowell, G. R., Falagush, O. and Yu, H.-S. 2012 'A particle refinement method for simulating DEM of cone penetration testing in granular materials', *Géotechnique Letters*, 2(3), pp. 141–147. doi: 10.1680/geolett.12.00036.

Mindlin, R. D. and Deresiewicz, H. 1953 'Elastic spheres in contact under varying oblique forces', *Journal of Applied Mechanics ASME*, 20, pp. 327–344. doi: 10.1007/978-1-4613-8865-4_35.

Mohajerani, A., Bosnjak, D. and Bromwich, D. 2014 'Analysis and design methods of screw piles: A review', *Soils and Foundations*, 1 February, pp. 115–128. doi: 10.1016/j.sandf.2016.01.009.

Perko, H. A. 2009 'Helical Piles', in *New Technological and Design Developments in Deep Foundations*. Denver: John Wiley & Sons, Inc. doi: 10.1002/9780470549063.

Richards, D., Blake, A., White, D. J., Bittar, E. M. and Lehane, B. M. 2019 'Field Tests Assessing the Installation Performance of Screw Pile Geometries Optimised for Offshore Wind Applications', in Davidson, C. ;, Brown, M. J., Knappett, J. A., Brennan, A. J., Augarde, C. E., Coombs, W. M., Wang, L.,

Richards, D., White, D. J., and Blake, A. (eds) *ISSPEA*. Dundee, UK: University of Dundee, pp. 47–54. doi: 10.20933/100001123.

Sharif, Y., Brown, M. J., Ciantia, M., Knappett, J., Davidson, C., Cerfontaine, B., Robinson, S. and Ball, J. 2019a 'Numerically Modelling the Installtion and loading of Screw Piles using DEM', in Davidson, C., Brown, M. J., Knappett, J. A., Brennan, A. J., Augarde, C. E., Coombs, W. M., Wang, L., Richards, D., White, D. J., and Blake, A. (eds) *International Symposium on Screw Piles for Energy Applications*. Dundee, UK: University of Dundee, pp. 101–108. doi: 10.20933/100001123.

Sharif, Y., Ciantia, M., Brown, M. J., Knappett, J. A. and Ball, J. D. 2019b 'Numerical Techniques For the Fast Generation of Samples Using the Particle Refinement Method', in *Proceedings of the 8th International Conference on Discrete Element Methods*. Enschede, Netherlands, p. 181.

Sharif, Y. U., Brown, M. J., Ciantia, M. O., Cerfontaine, B., Davidson, C., Knappett, J., Meijer, G. J. and Ball, J. 2020 'Using DEM to create a CPT based method to estimate the installation requirements of rotary installed piles in sand', *Canadian Geotechnical Journal published online 19/08/2020*. doi: <http://dx.doi.org/10.1139/cgj-2020-0017>.

Shi, D., Yang, Y., Deng, Y. and Liu, W.-B. 2018 'Experimental study of the effect of drilling velocity ratio on the behavior of auger piling in sand.', *Rock and Soil Mechanics*, 39(6), pp. 1981–1990. doi: 10.16285/j.rsm.2017.1900 (In Chinese).

Shi, D., Yang, Y., Deng, Y. and Xue, J. 2019 'DEM modelling of screw pile penetration in loose granular assemblies considering the effect of drilling velocity ratio', *Granular Matter*. Springer Berlin Heidelberg, 21(3), pp. 1–16. doi: 10.1007/s10035-019-0933-3.

Tappenden, K. and Sego, D. 2007 'Predicting the axial capacity of screw piles installed in Canadian soils', in *60th Canadian Geotechnical Conference*. Ottawa, Ontario, Canada, pp. 1608–1615.

Terzaghi, K. (1939) 'Soil Mechanics: a new chapter in engineering science', *Journal of the Institution of Civil Engineers*, 12(7), pp. 106–141.

Tsuha, C. de H. C. and Aoki, N. 2010 'Relationship between installation torque and uplift capacity of deep helical piles in sand', *Canadian Geotechnical Journal*, 47(6), pp. 635–647. doi: 10.1139/T09-128.

Viggiani, C. 1989 'Influenza dei fattori tecnologici sul comportamento dei pali.', in *Atti, XVII Convegno Nazionale di Geotecnica*. Taormina, pp. 83–91.(In Italian)

Zhang, N., Arroyo, M., Ciantia, M. O., Gens, A. and Butlanska, J. 201) 'Standard penetration testing in a virtual calibration chamber', *Computers and Geotechnics*, 111, pp. 277–289. doi:

10.1016/j.compgeo.2019.03.021.

7 Notation list

AR	Advancement ratio
CFA	Continuous flight auger
CPT	Cone penetration test
CRP	Constant rate of penetration
d_{100}	largest particle diameter
d_{50}	median particle diameter
D_c	Diameter of screw pile central core
DEM	Discrete element method
D_h	Diameter of screw pile helix
D_r	Relative density
G	Hertz shear modulus (inter-particle contact model)
G_{pile}	Hertz shear modulus (interface contact model)
h	Depth below ground surface
H	Embedment depth from soil surface to mid-helix height
K	Empirical torque correlation factor
K^*	Dimensionless empirical torque correlation factor
L	Total Length of screw pile
L_p	Width of plastic deformation zone
L_{pr}	Width of plastic deformation zone to determine the rotational velocity
L_{pv}	Width of plastic deformation zone to determine the vertical velocity
n	Rotation rate
n_i	Particle scaling value
N	Centrifuge model scaling value
p'	Mean effective stress
p_0'	Initial mean effective stress
PCRM	Periodic cell replication method
P_h	Geometric pitch of screw pile helix
PRM	Particle refinement method
PSD	Particle size distribution
Q_c	Ultimate compressive capacity
Q_t	Ultimate tensile capacity
r	Radial distance from centre
REV	Representative element volume
T	Total installation torque
U	Average Particle displacement
v_{crit}	Critical drill velocity for a CFA pile
y	Vertical displacement during axial loading
z	Penetration depth
γ'	Effective unit weight of soil
Δz	Displacement for single rotation
δh	Vertical particle displacement
δr	Radial particle displacement
μ	Inter-particle friction coefficient
μ_{pile}	Interface friction coefficient

ν	Poisson's ratio (inter-particle contact model)
ν	Poisson' ratio (interface contact model)
ρ	Density of particles
σ_v	Vertical stress in soil
$\dot{\gamma}$	Shear strain rate
$\dot{\theta}$	Rotational velocity
\dot{w}	Vertical velocity of pile

8 Table caption list

Table 1: HST95 sand physical and numerical properties (Sharif et al 2019a)

Table 2: Properties of soil beds used in this study at different relative densities (model scale parameters)

9 Figure caption list

Figure 1: Schematic diagram of screw pile used in this study, a) geometric properties, b) screw pile prototype dimensions. (model dimensions in brackets)

Figure 2: Example soil bed used in this study, screw pile installed to full embedment depth, 40m (0.5m) diameter and 32m (0.4m) in height. Particle shading indicates particle size distribution scaling applied ($D_r = 83\%$, $AR = 0.5$)

Figure 3: Installation requirements with depth of screw pile installed at varying advancement ratios. a) Compressive installation force ($D_r = 30\%$) b) Installation torque($D_r = 30\%$), c) Compressive installation force ($D_r = 52\%$) d) Installation torque($D_r = 52\%$), e) Compressive installation force ($D_r = 83\%$) f) Installation torque($D_r = 83\%$)

Figure 4: Evolution of advancement ratio (AR) with depth for a self-weight installed pile installed into a dense sand bed ($D_r = 83\%$).

Figure 5: Post installation axial capacity against normalised displacement. a) Compressive capacity ($D_r = 30\%$) b) Tensile capacity ($D_r = 30\%$), c) Compressive capacity ($D_r = 52\%$) d) Tensile capacity ($D_r = 52\%$), e) Compressive capacity ($D_r = 83\%$) from *DEM* study and pitched match installation results from Davidson et al. (2020) f) Tensile capacity ($D_r = 83\%$) from *DEM* study and pitched match installation results from Davidson et al. (2020)

Figure 6: Normalised results of the effects on advancement ratio and relative density on screw pile in-service performance. a) Compressive installation force, b) Installation torque, c) Compressive capacity, d) Tensile capacity. (Data at 1.0, 1.0 is offset for each relative density to allow distinction of data points)

Figure 7: Diagram of mechanism produced for different advancement ratios during tensile uplift testing in loose sand bed ($D_r = 32\%$). a) $AR = 0.5$, b) $AR = 1.0$, c) Change in relative density d) Change in relative density

Figure 8: Approximated failure surfaces calculated using the relative density index (Bolton, 1986) (left: Initial soil conditions, right: post installation conditions), superimposed over a diagram of the uplift mechanism of screw piles installed at different advancement ratios ($D_r = 83\%$) (screw pile is shown in its final position). a) $AR = 0.5$ b) $AR = 1.0$

Figure 9: Back calculated torque-capacity correlation factors compared to Equation 2 (Perko 2009) and centrifuge study of Davidson et al (2020) a) Tensile K_t b) compressive K_c

Figure 10: Residual locked in stresses at the end of installation produced by different advancement ratios

Figure 11: Comparison of particle displacement during installation between pitch matched ($AR = 1.0$) and over flighted ($AR = 0.5$) installation a) vertical displacement b) radial displacement

Figure 12: Dimensionless torque correlation factors back calculated using equation 3 in accordance with Byrne and Houlsby (2015) a) Tensile K_t^* , b) Compressive K_c^*

Figure 13: Mechanism form for installed screw piles during axial capacity testing ($AR=0.5$) a) compression ($H/D_h = 7$) b) tension ($H/D_h = 7$) c) compression ($H/D_h = 11$) d) tension ($H/D_h = 11$)

Figure 14: The effect of relative embedment depth and advancement ratio on torque-capacity correlation factors in a dense soil bed. a) Tension b) Compression

Draft

Table 1: HST95 sand physical and numerical properties (Sharif et al 2019a)

HST95 silica sand property	Value
<i>Physical properties</i>	
Sand unit weight γ (kN/m ³)	16.75
Minimum dry density γ_{\max} (kN/m ³)	14.59
Maximum dry density γ_{\min} (kN/m ³)	17.58
Critical state friction angle, ϕ (degrees)	32
Interface friction angle, δ (degrees)	18
D ₃₀ (mm)	0.12
D ₆₀ (mm)	0.14
<i>DEM Parameters</i>	
Shear modulus, G (GPa)	3
Friction coefficient, μ (-)	0.264
Poisson's ratio, ν (-)	0.3
Interface friction coefficient [pile], μ_{pile} (-)	0.16

Table 2: Properties of soil beds used in this study at different relative densities (model scale parameters)

Property	Loose	Medium Dense	Dense
Relative Density (%)	30	52	83
Voids ratio (e)	0.68	0.61	0.52
Height (mm)	400	400	400
Radius (mm)	250	250	250
Core PSD scaling (N _c)	20	20	20
Gravitational field	48	48	48
Number of Particles	190,000	220,000	270,000
Formation time	30 hours	25 hours	22 hours

Draft

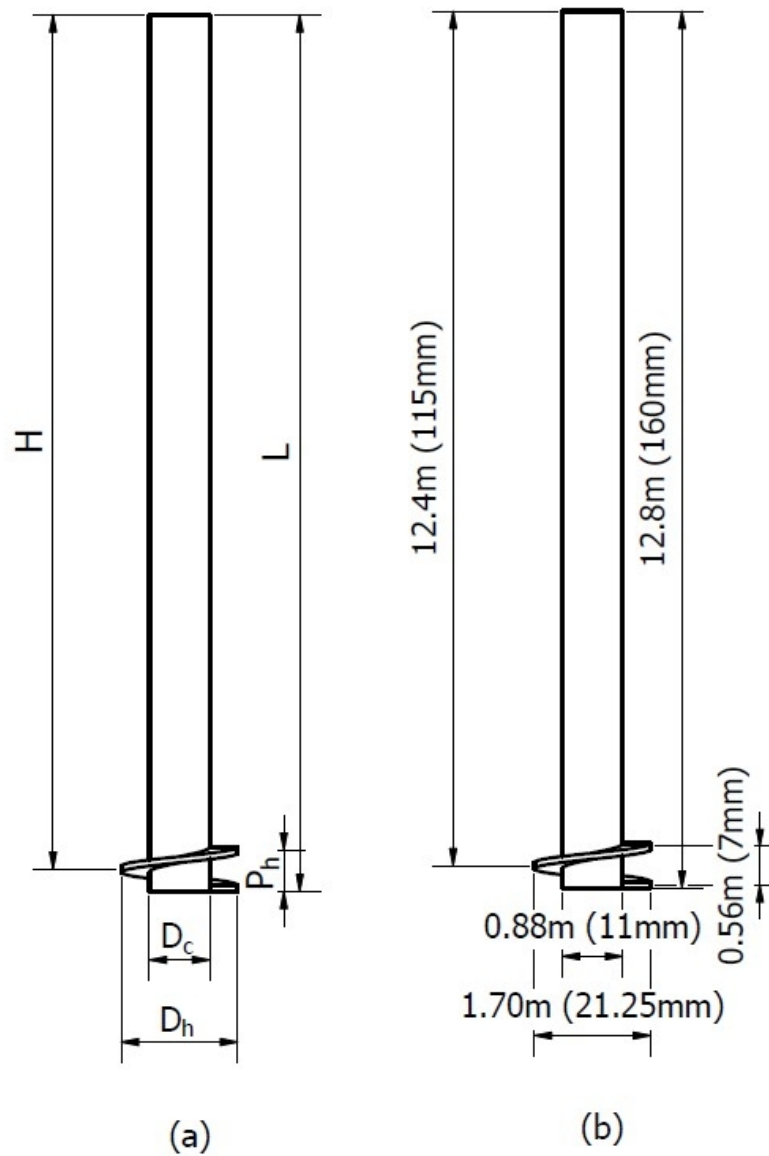


Figure 1: Schematic diagram of screw pile used in this study, a) geometric properties, b) screw pile prototype dimensions. (model dimensions in brackets)

138x200mm (96 x 96 DPI)

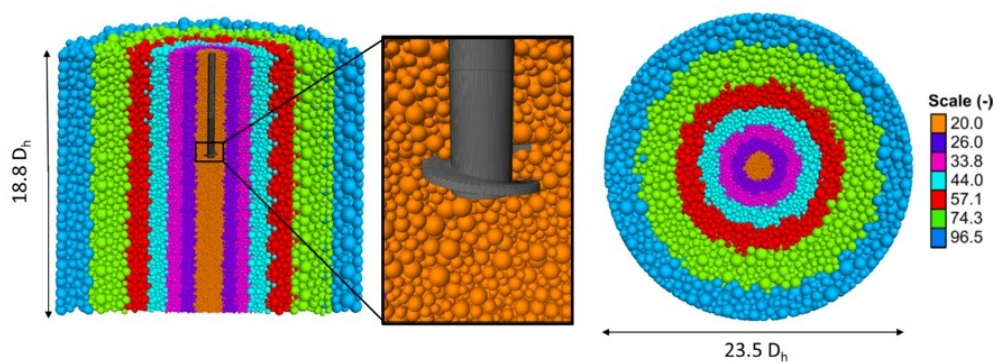


Figure 2: Example soil bed used in this study, screw pile installed to full embedment depth, 40m (0.5m) diameter and 32m (0.4m) in height. Particle shading indicates particle size distribution scaling applied ($D_r = 83\%$, $AR = 0.5$)

150x56mm (150 x 150 DPI)

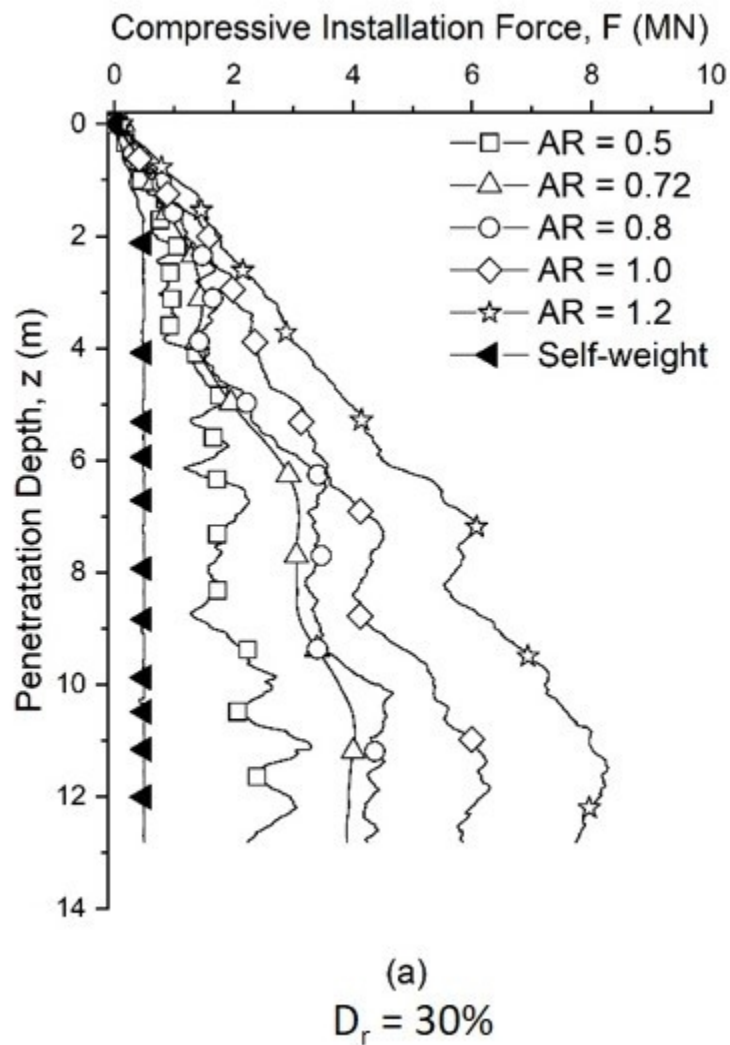


Figure 3: Installation requirements with depth of screw pile installed at varying advancement ratios. a) Compressive installation force ($D_r = 30\%$) b) Installation torque ($D_r = 30\%$), c) Compressive installation force ($D_r = 52\%$) d) Installation torque ($D_r = 52\%$), e) Compressive installation force ($D_r = 83\%$) f) Installation torque ($D_r = 83\%$)

74x93mm (150 x 150 DPI)

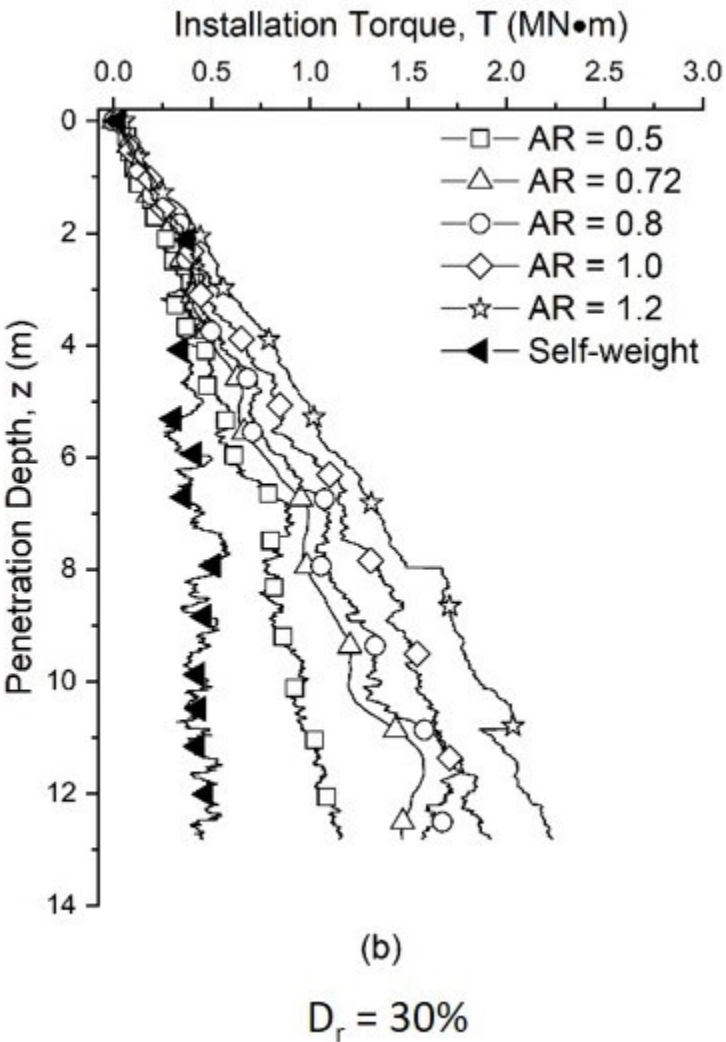


Figure 3: Installation requirements with depth of screw pile installed at varying advancement ratios. a) Compressive installation force ($D_r = 30\%$) b) Installation torque ($D_r = 30\%$), c) Compressive installation force ($D_r = 52\%$) d) Installation torque ($D_r = 52\%$), e) Compressive installation force ($D_r = 83\%$) f) Installation torque($D_r = 83\%$)

75x93mm (150 x 150 DPI)

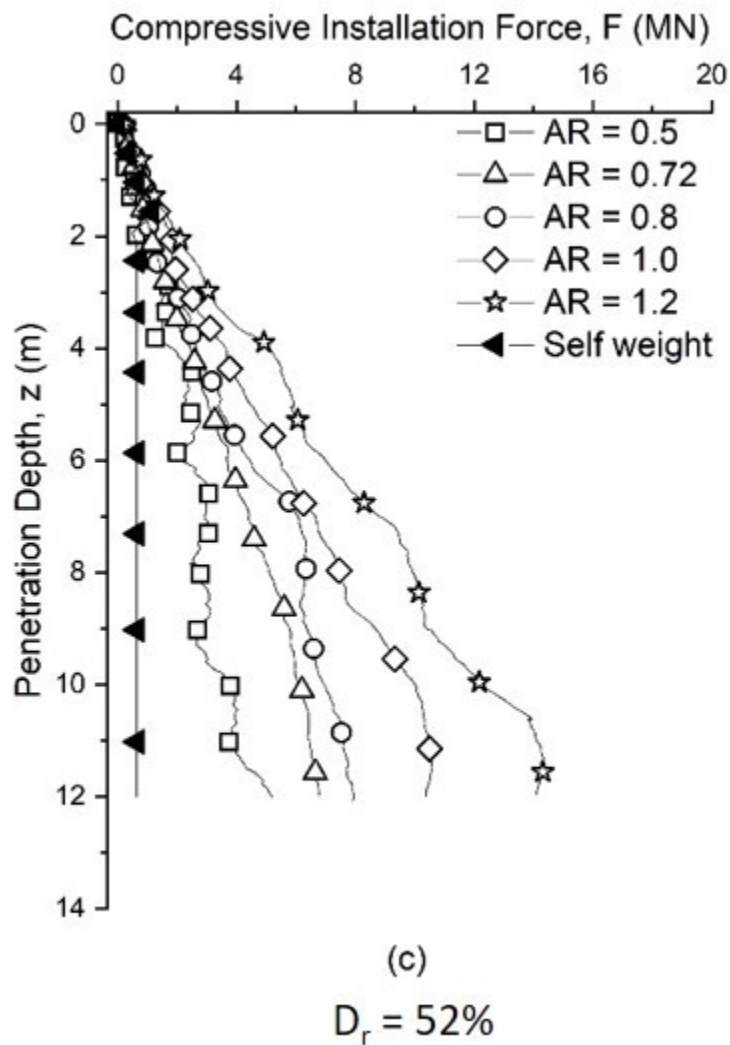


Figure 3: Installation requirements with depth of screw pile installed at varying advancement ratios. a) Compressive installation force ($D_r = 30\%$) b) Installation torque ($D_r = 30\%$), c) Compressive installation force ($D_r = 52\%$) d) Installation torque ($D_r = 52\%$), e) Compressive installation force ($D_r = 83\%$) f) Installation torque ($D_r = 83\%$)

75x93mm (150 x 150 DPI)

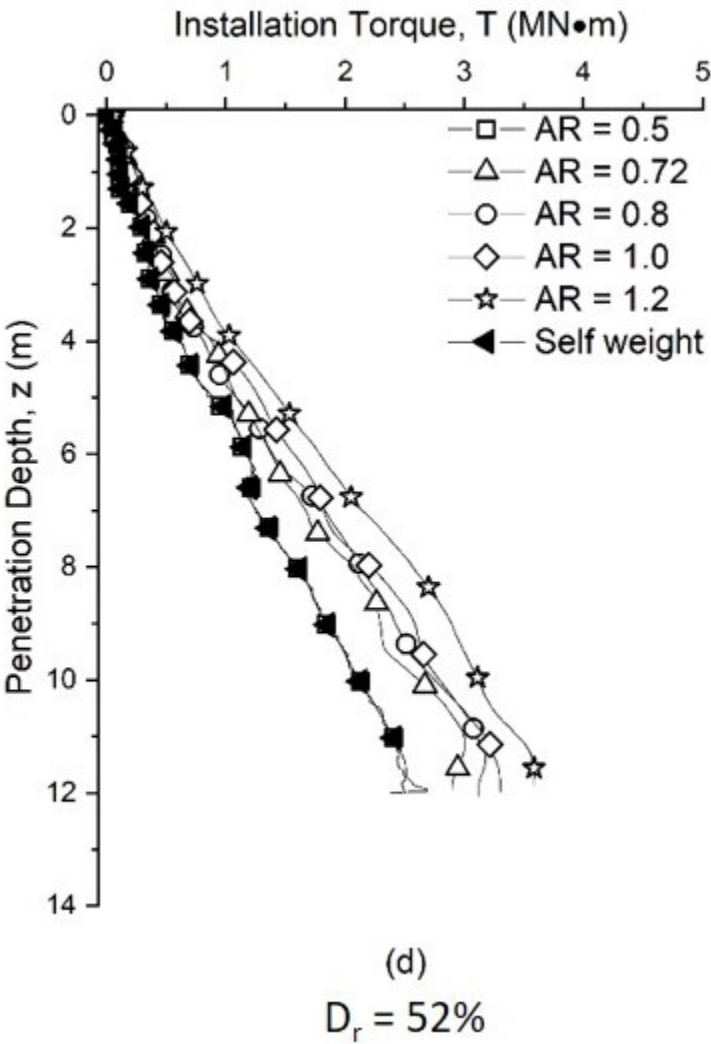


Figure 3: Installation requirements with depth of screw pile installed at varying advancement ratios. a) Compressive installation force ($D_r = 30\%$) b) Installation torque ($D_r = 30\%$), c) Compressive installation force ($D_r = 52\%$) d) Installation torque ($D_r = 52\%$), e) Compressive installation force ($D_r = 83\%$) f) Installation torque($D_r = 83\%$)

75x93mm (150 x 150 DPI)

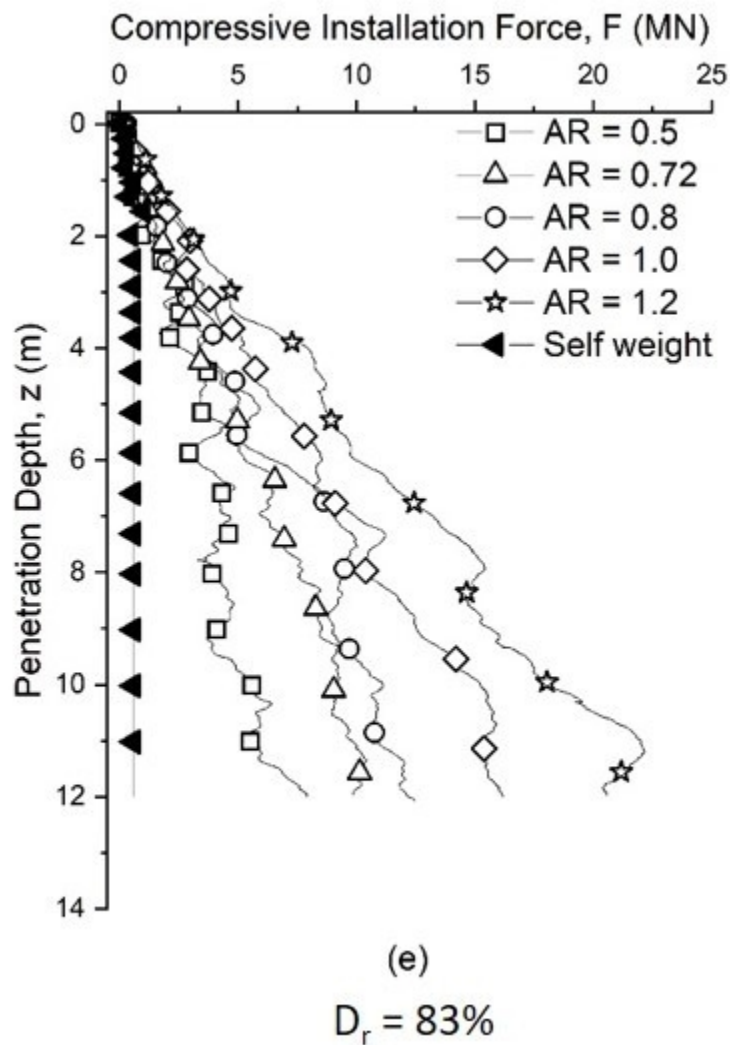
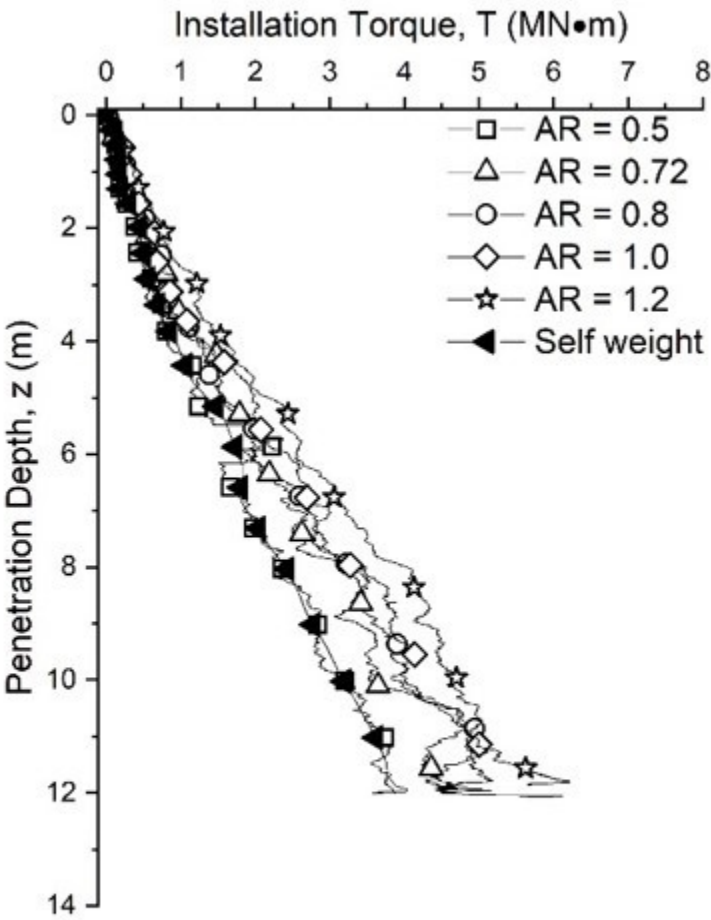


Figure 3: Installation requirements with depth of screw pile installed at varying advancement ratios. a) Compressive installation force ($D_r = 30\%$) b) Installation torque ($D_r = 30\%$), c) Compressive installation force ($D_r = 52\%$) d) Installation torque ($D_r = 52\%$), e) Compressive installation force ($D_r = 83\%$) f) Installation torque ($D_r = 83\%$)

75x93mm (150 x 150 DPI)



(f)
 $D_r = 83\%$

Figure 3: Installation requirements with depth of screw pile installed at varying advancement ratios. a) Compressive installation force ($D_r = 30\%$) b) Installation torque ($D_r = 30\%$), c) Compressive installation force ($D_r = 52\%$) d) Installation torque ($D_r = 52\%$), e) Compressive installation force ($D_r = 83\%$) f) Installation torque($D_r = 83\%$)

75x93mm (150 x 150 DPI)

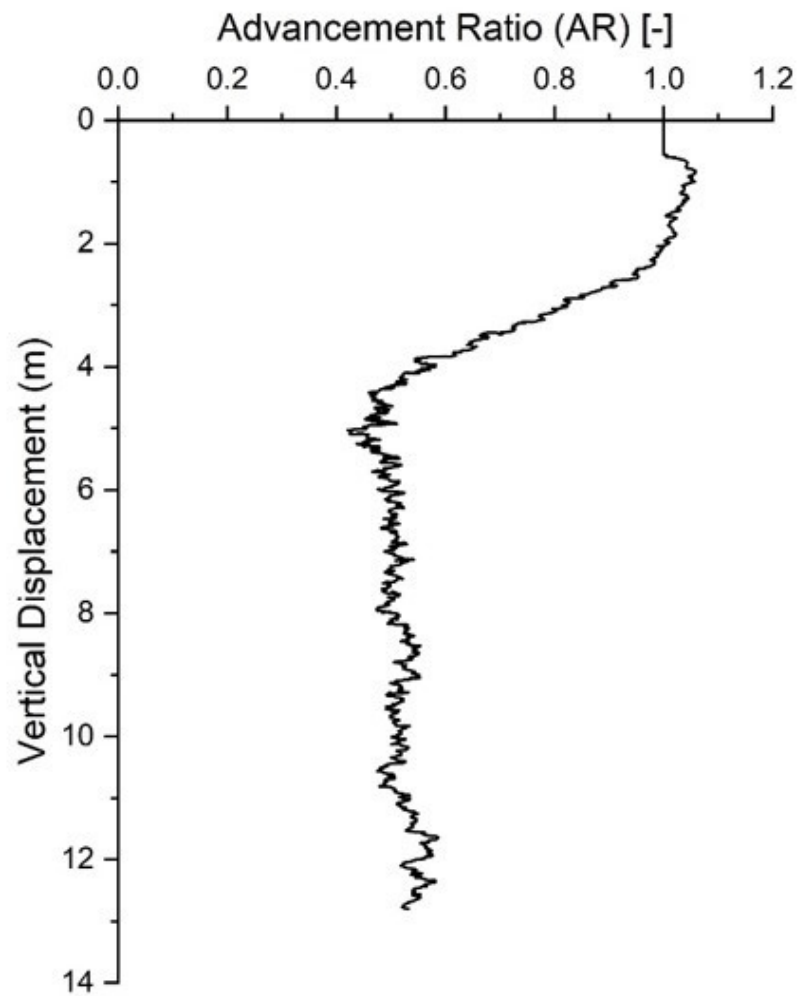


Figure 4: Evolution of advancement ratio (AR) with depth for a self-weight installed pile installed into a dense sand bed ($D_r = 83\%$).

85x107mm (150 x 150 DPI)

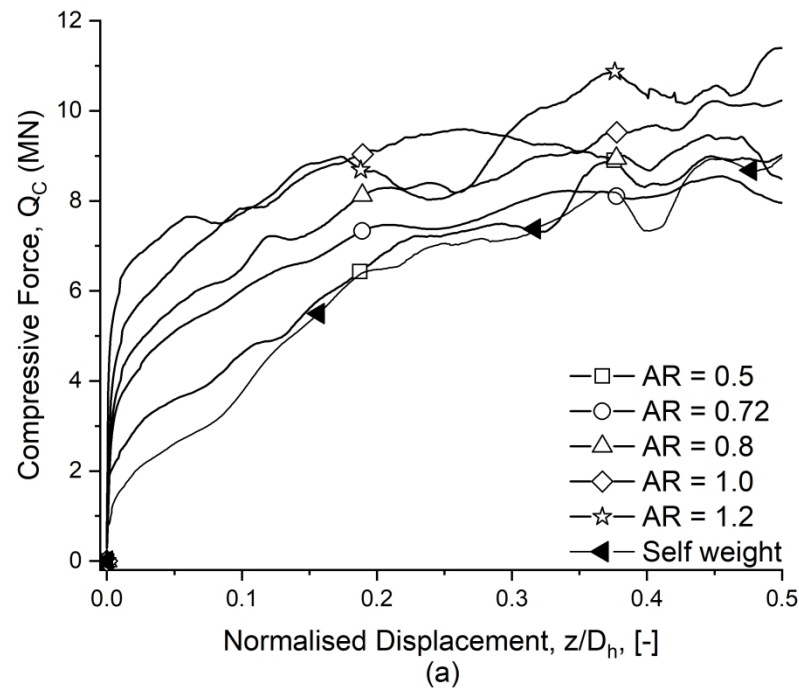


Figure 5: Post installation axial capacity against normalised displacement. a) Compressive capacity ($D_r = 30\%$) b) Tensile capacity ($D_r = 30\%$), c) Compressive capacity ($D_r = 52\%$) d) Tensile capacity ($D_r = 52\%$), e) Compressive capacity ($D_r = 83\%$) from DEM study and pitched-match installation results from Davidson et al. (2020) f) Tensile capacity ($D_r = 83\%$) from DEM study and pitched-match installation results from Davidson et al. (2020)

272x208mm (300 x 300 DPI)

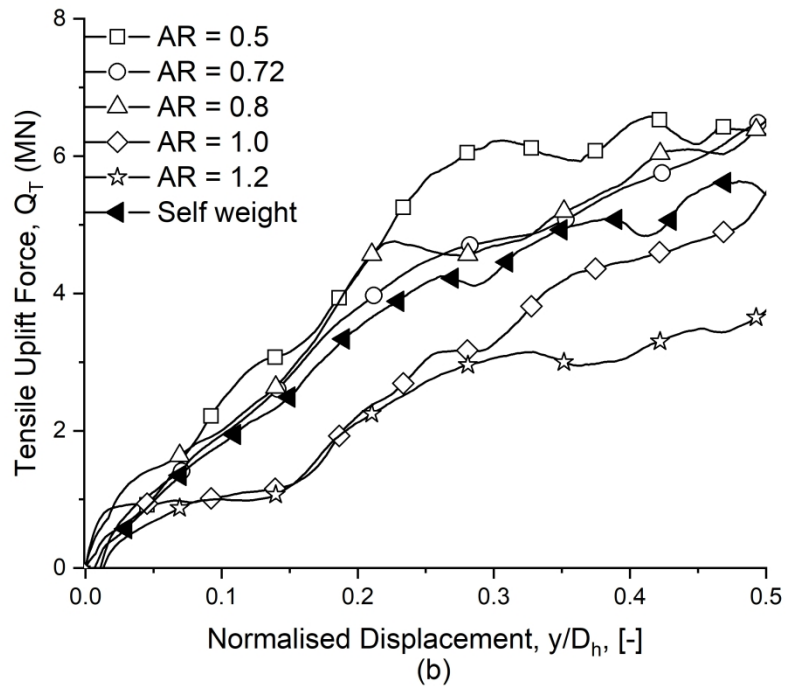


Figure 5: Post installation axial capacity against normalised displacement. a) Compressive capacity ($D_r = 30\%$) b) Tensile capacity ($D_r = 30\%$), c) Compressive capacity ($D_r = 52\%$) d) Tensile capacity ($D_r = 52\%$), e) Compressive capacity ($D_r = 83\%$) from DEM study and pitched-match installation results from Davidson et al. (2020) f) Tensile capacity ($D_r = 83\%$) from DEM study and pitched-match installation results from Davidson et al. (2020)

272x208mm (300 x 300 DPI)

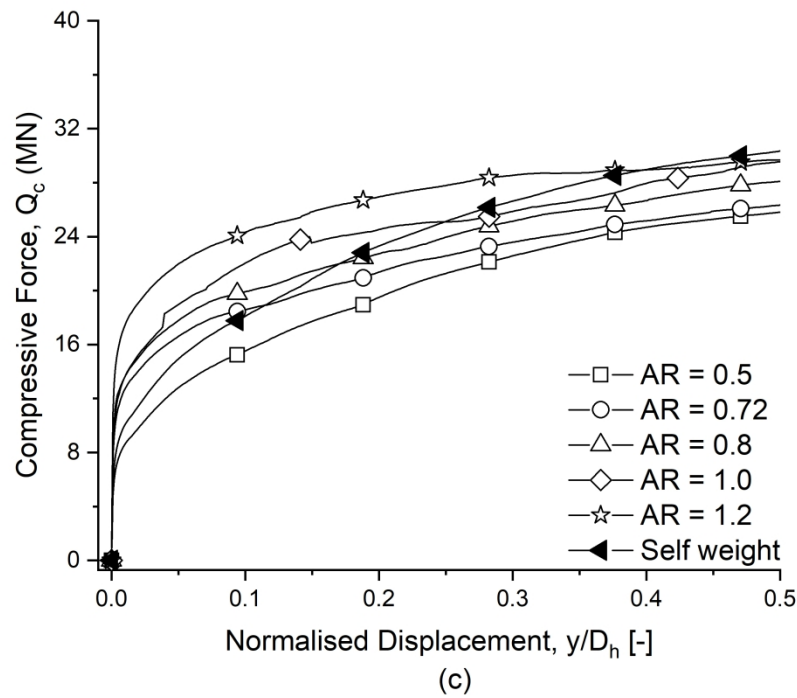


Figure 5: Post installation axial capacity against normalised displacement. a) Compressive capacity ($D_r = 30\%$) b) Tensile capacity ($D_r = 30\%$), c) Compressive capacity ($D_r = 52\%$) d) Tensile capacity ($D_r = 52\%$), e) Compressive capacity ($D_r = 83\%$) from DEM study and pitched-match installation results from Davidson et al. (2020) f) Tensile capacity ($D_r = 83\%$) from DEM study and pitched-match installation results from Davidson et al. (2020)

272x208mm (300 x 300 DPI)

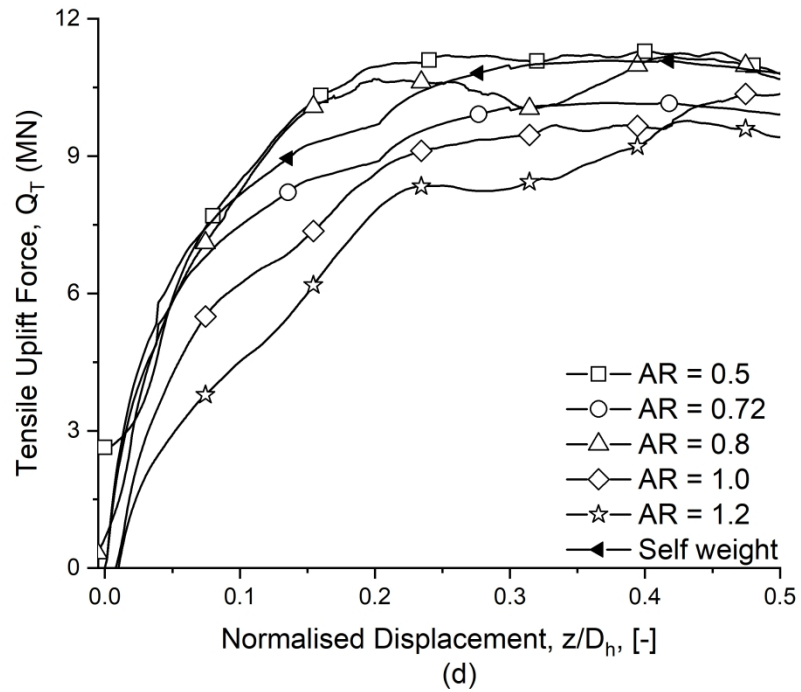


Figure 5: Post installation axial capacity against normalised displacement. a) Compressive capacity ($D_r = 30\%$) b) Tensile capacity ($D_r = 30\%$), c) Compressive capacity ($D_r = 52\%$) d) Tensile capacity ($D_r = 52\%$), e) Compressive capacity ($D_r = 83\%$) from DEM study and pitched-match installation results from Davidson et al. (2020) f) Tensile capacity ($D_r = 83\%$) from DEM study and pitched-match installation results from Davidson et al. (2020)

272x208mm (300 x 300 DPI)

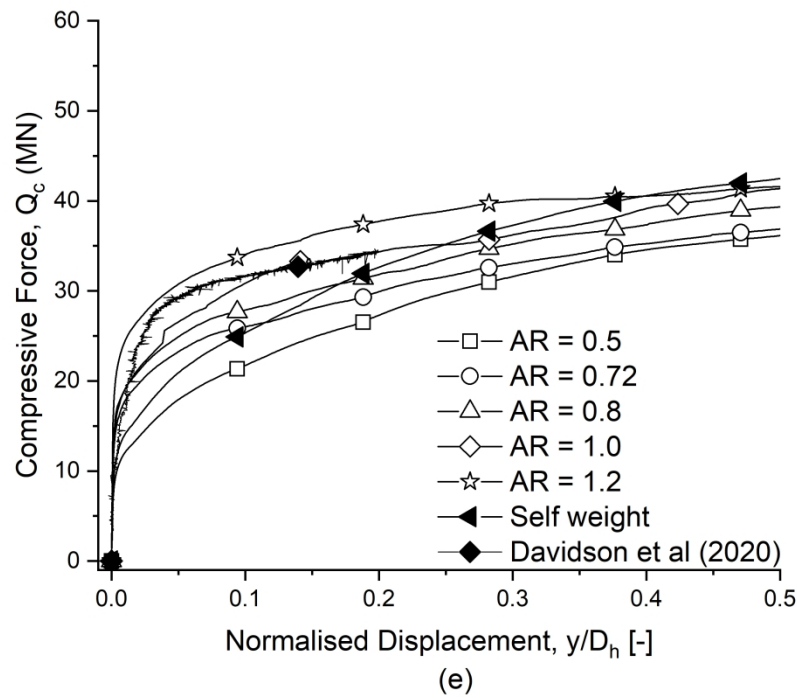


Figure 5: Post installation axial capacity against normalised displacement. a) Compressive capacity ($D_r = 30\%$) b) Tensile capacity ($D_r = 30\%$), c) Compressive capacity ($D_r = 52\%$) d) Tensile capacity ($D_r = 52\%$), e) Compressive capacity ($D_r = 83\%$) from DEM study and pitched-match installation results from Davidson et al. (2020) f) Tensile capacity ($D_r = 83\%$) from DEM study and pitched-match installation results from Davidson et al. (2020)

272x208mm (300 x 300 DPI)

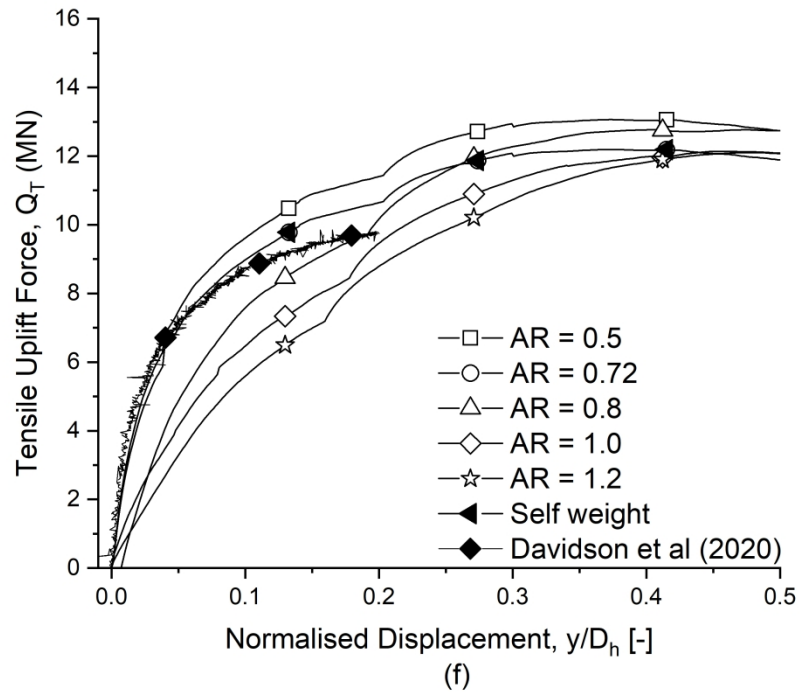


Figure 5: Post installation axial capacity against normalised displacement. a) Compressive capacity ($D_r = 30\%$) b) Tensile capacity ($D_r = 30\%$), c) Compressive capacity ($D_r = 52\%$) d) Tensile capacity ($D_r = 52\%$), e) Compressive capacity ($D_r = 83\%$) from DEM study and pitched-match installation results from Davidson et al. (2020) f) Tensile capacity ($D_r = 83\%$) from DEM study and pitched-match installation results from Davidson et al. (2020)

272x208mm (300 x 300 DPI)

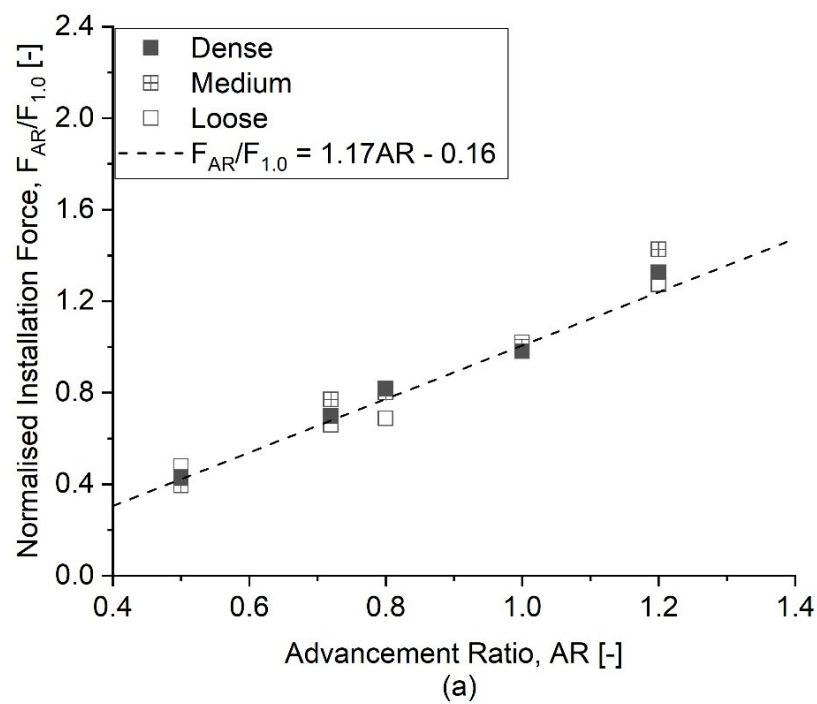


Figure 6: Normalised results of the effects on advancement ratio and relative density on screw pile in-service performance. a) Compressive installation force, b) Installation torque, c) Compressive capacity, d) Tensile capacity. (Data at 1.0, 1.0 is offset for each relative density to allow distinction of data points)

130x99mm (220 x 220 DPI)

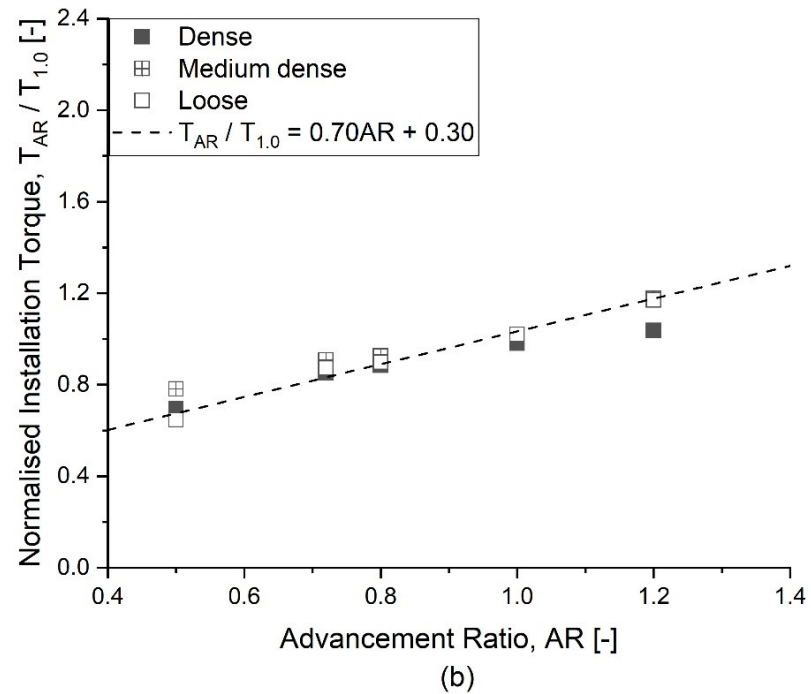


Figure 6: Normalised results of the effects on advancement ratio and relative density on screw pile in-service performance. a) Compressive installation force, b) Installation torque, c) Compressive capacity, d) Tensile capacity. (Data at 1.0, 1.0 is offset for each relative density to allow distinction of data points)

130x99mm (220 x 220 DPI)

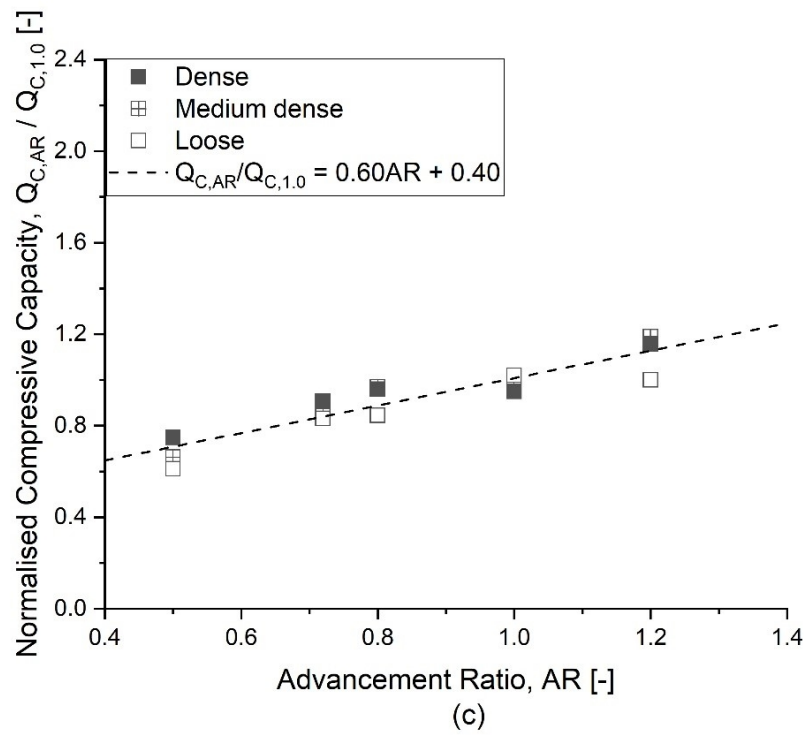


Figure 6: Normalised results of the effects on advancement ratio and relative density on screw pile in-service performance. a) Compressive installation force, b) Installation torque, c) Compressive capacity, d) Tensile capacity. (Data at 1.0, 1.0 is offset for each relative density to allow distinction of data points)

130x99mm (220 x 220 DPI)

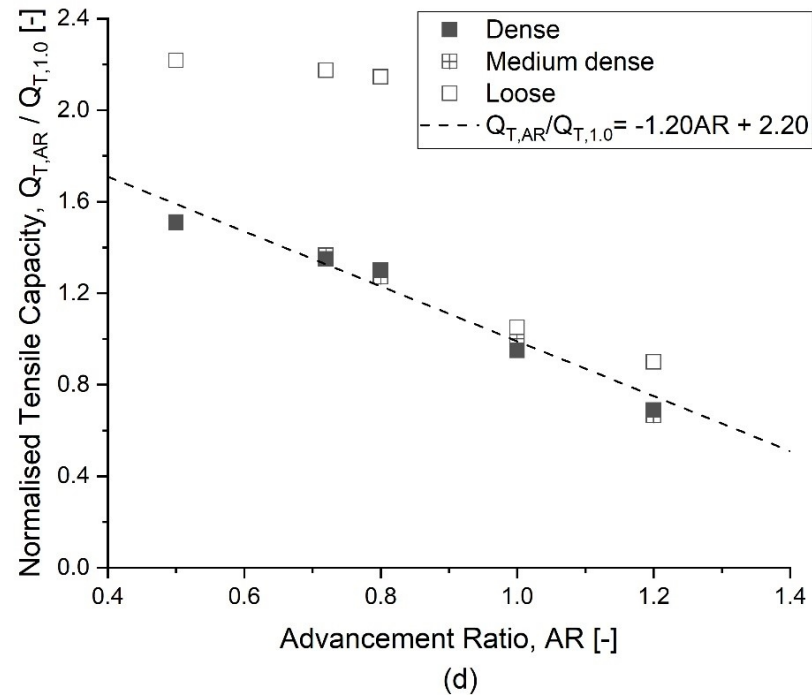


Figure 6: Normalised results of the effects on advancement ratio and relative density on screw pile in-service performance. a) Compressive installation force, b) Installation torque, c) Compressive capacity, d) Tensile capacity. (Data at 1.0, 1.0 is offset for each relative density to allow distinction of data points)

130x99mm (220 x 220 DPI)

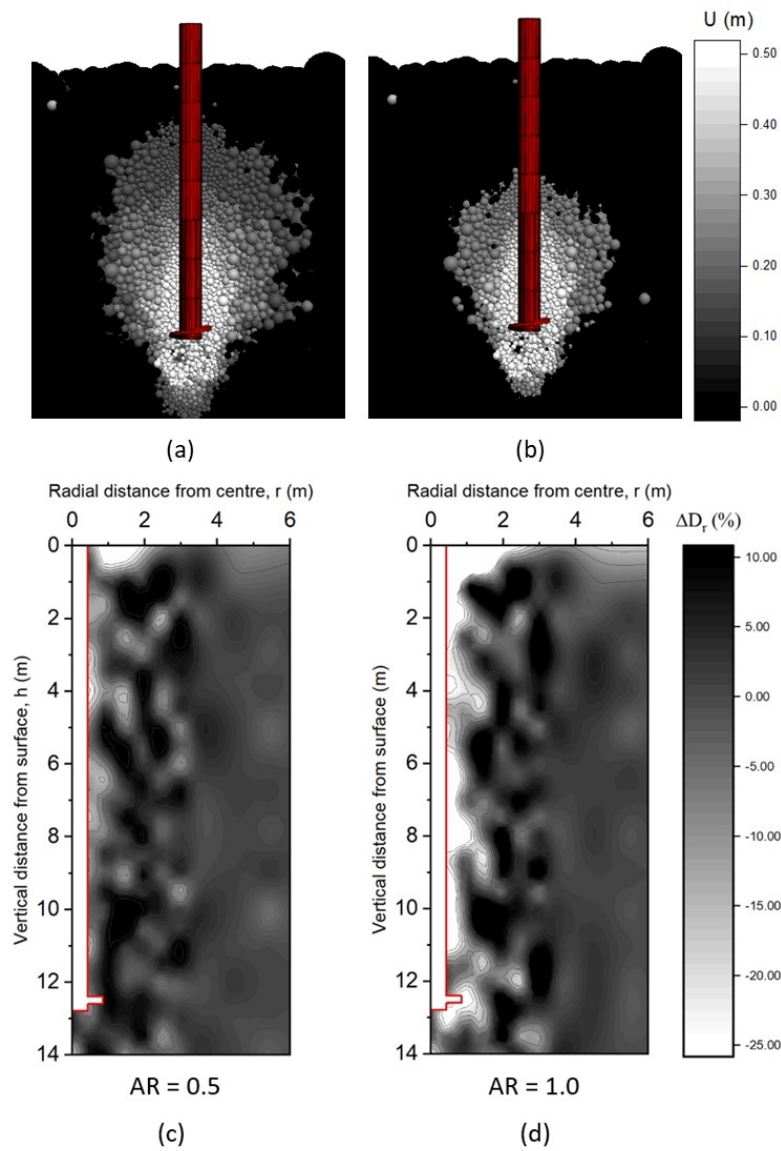


Figure 7: Diagram of mechanism produced for different advancement ratios during tensile uplift testing in loose sand bed ($D_r = 32\%$). a) $AR = 0.5$, b) $AR = 1.0$, c) Change in relative density d) Change in relative density

143x193mm (150 x 150 DPI)

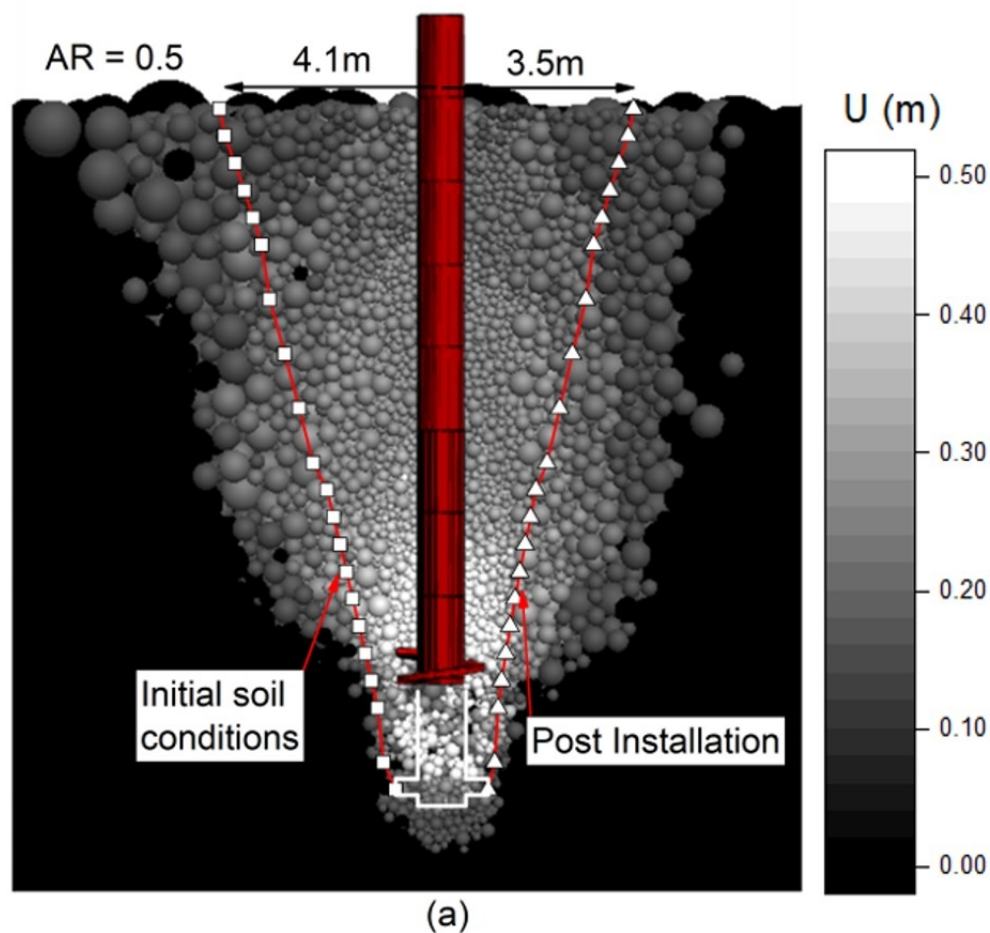


Figure 8: Approximated failure surfaces calculated using the relative density index (Bolton, 1986) (left: Initial soil conditions, right: post installation conditions), superimposed over a diagram of the uplift mechanism of screw piles installed at different advancement ratios ($D_r = 83\%$) (screw pile is shown in its final position). a) AR = 0.5 b) AR = 1.0

158x149mm (150 x 150 DPI)

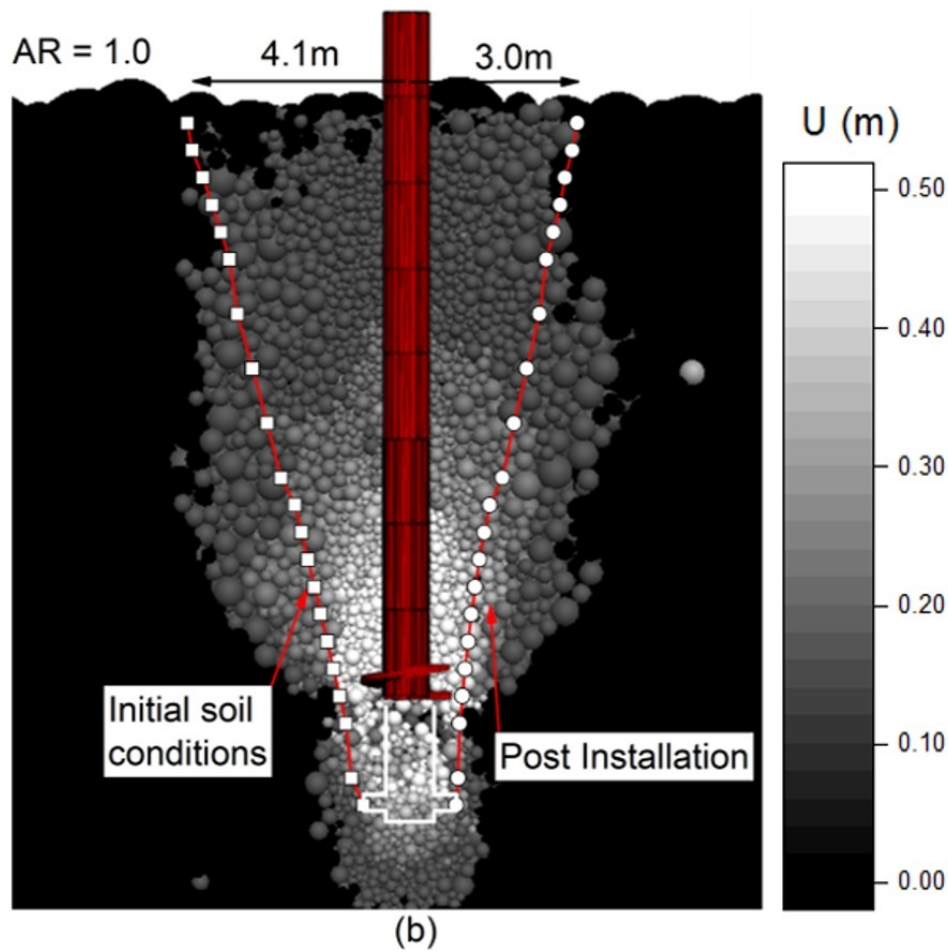


Figure 8: Approximated failure surfaces calculated using the relative density index (Bolton, 1986) (left: Initial soil conditions, right: post installation conditions), superimposed over a diagram of the uplift mechanism of screw piles installed at different advancement ratios ($D_r = 83\%$) (screw pile is shown in its final position). a) $AR = 0.5$ b) $AR = 1.0$

157x149mm (150 x 150 DPI)

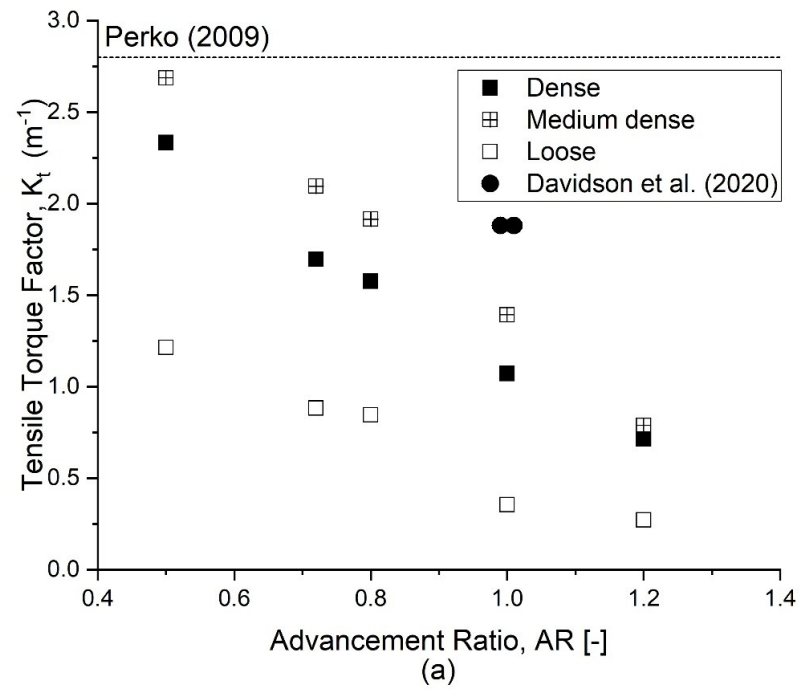


Figure 9: Back calculated torque-capacity correlation factors compared to Equation 2 (Perko 2009) and centrifuge study of Davidson et al (2020) a) Tensile K_t b) compressive K_c

143x110mm (220 x 220 DPI)

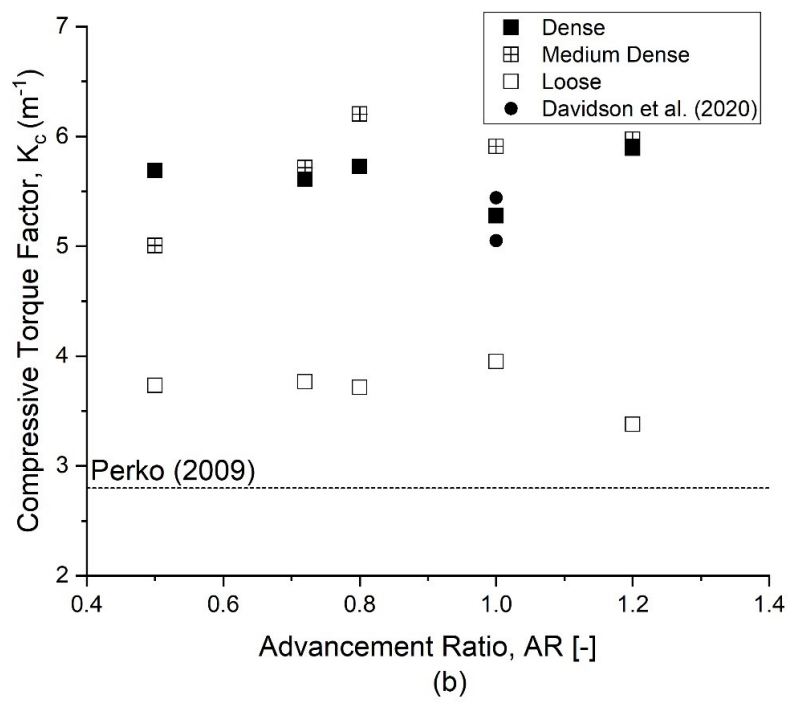


Figure 9: Back calculated torque-capacity correlation factors compared to Equation 2 (Perko 2009) and centrifuge study of Davidson et al (2020) a) Tensile K_t b) compressive K_c

143x110mm (220 x 220 DPI)

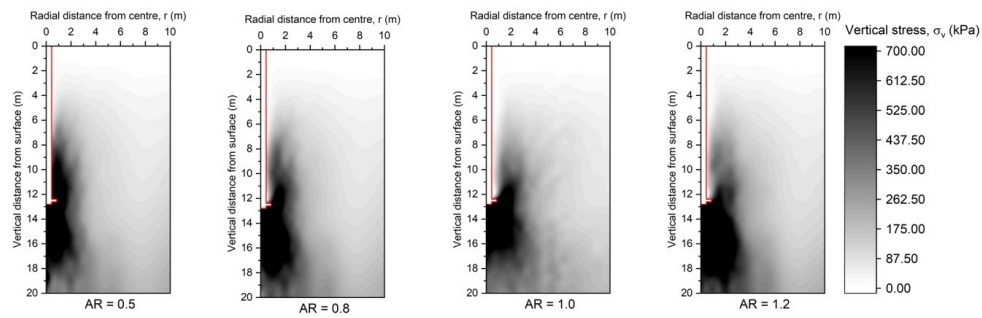


Figure 10: Residual locked in stresses at the end of installation produced by different advancement ratios

362x122mm (96 x 96 DPI)

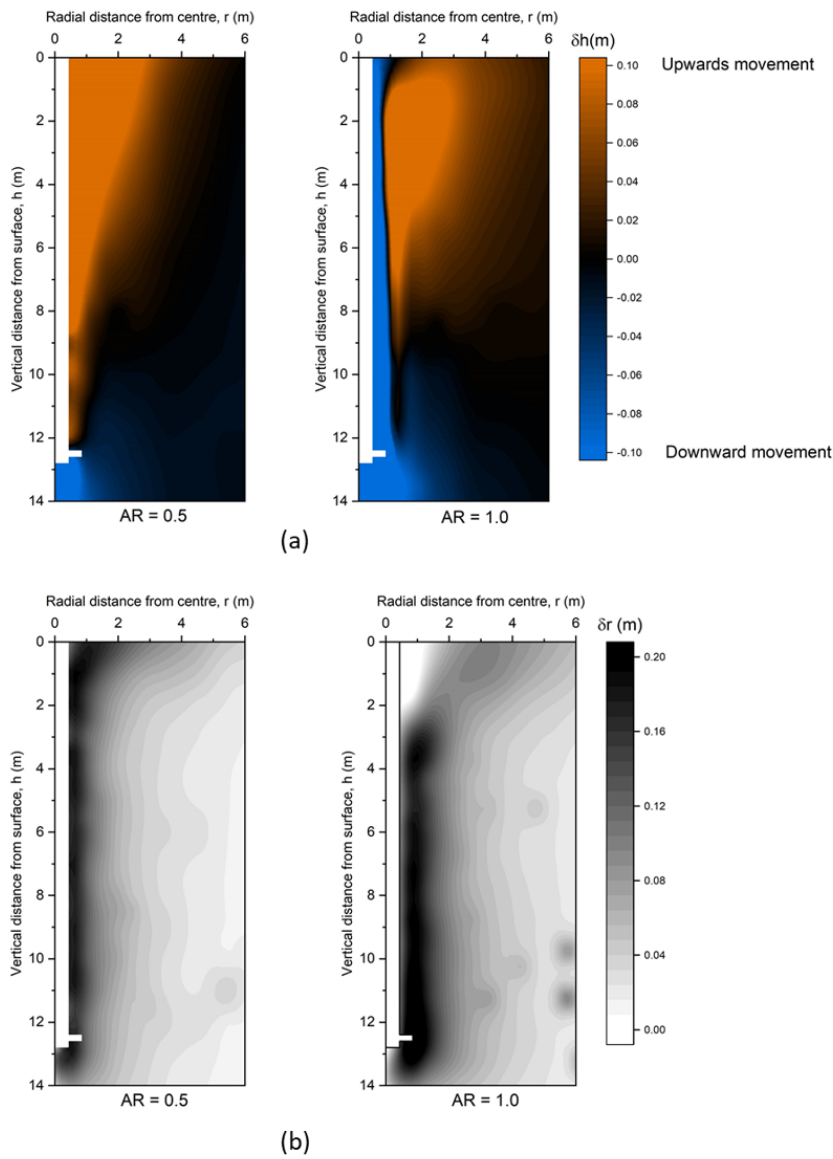


Figure 11: Comparison of particle displacement during installation between pitch matched (AR = 1.0) and over-flighted (AR = 0.5) installation a) vertical displacement b) radial displacement

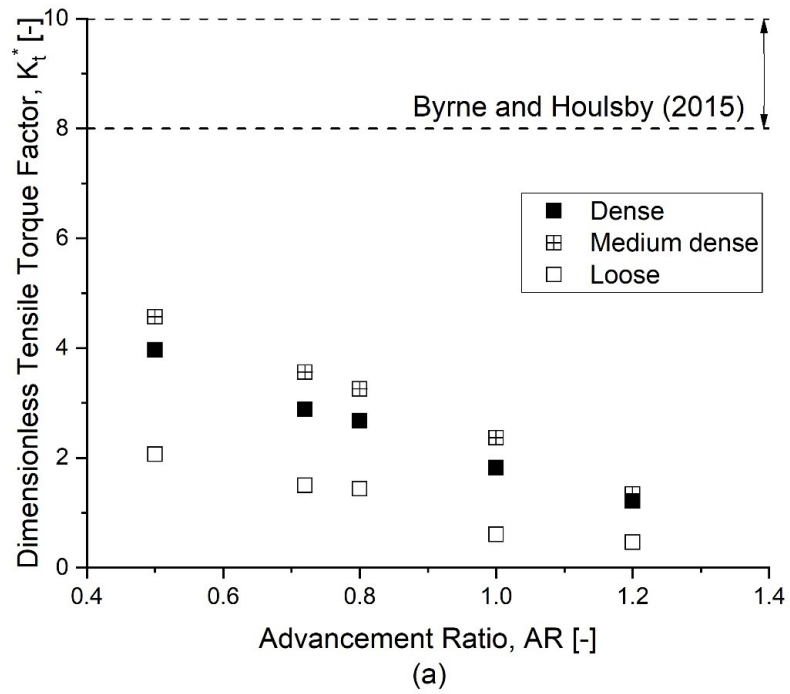


Figure 12: Dimensionless torque correlation factors back calculated using equation 3 in accordance with Byrne and Houlsby (2015) a) Tensile K_t^* , b) Compressive K_c^*

149x114mm (220 x 220 DPI)

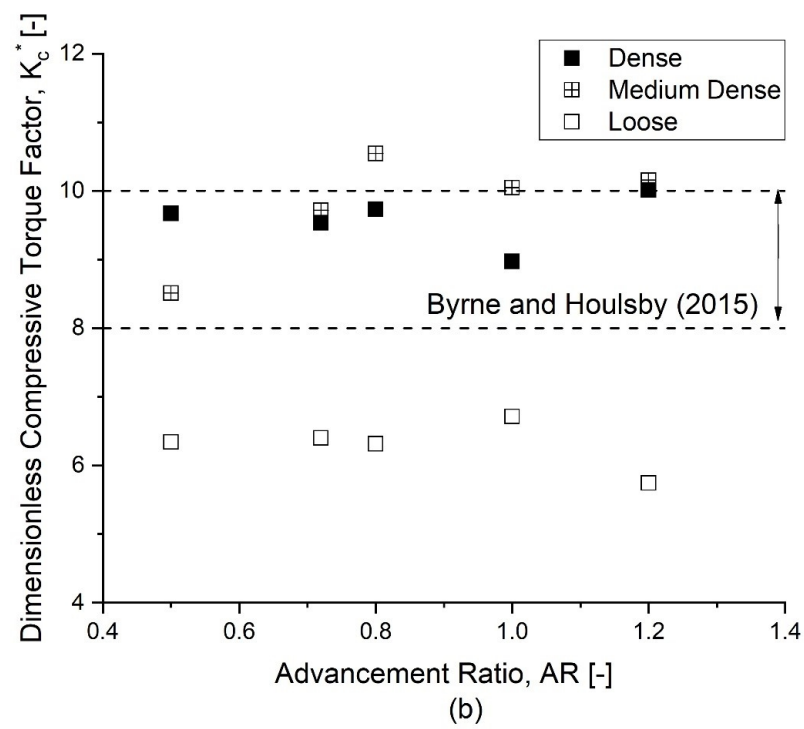


Figure 12: Dimensionless torque correlation factors back calculated using equation 3 in accordance with Byrne and Houlsby (2015) a) Tensile K_t^* , b) Compressive K_c^*

149x114mm (220 x 220 DPI)

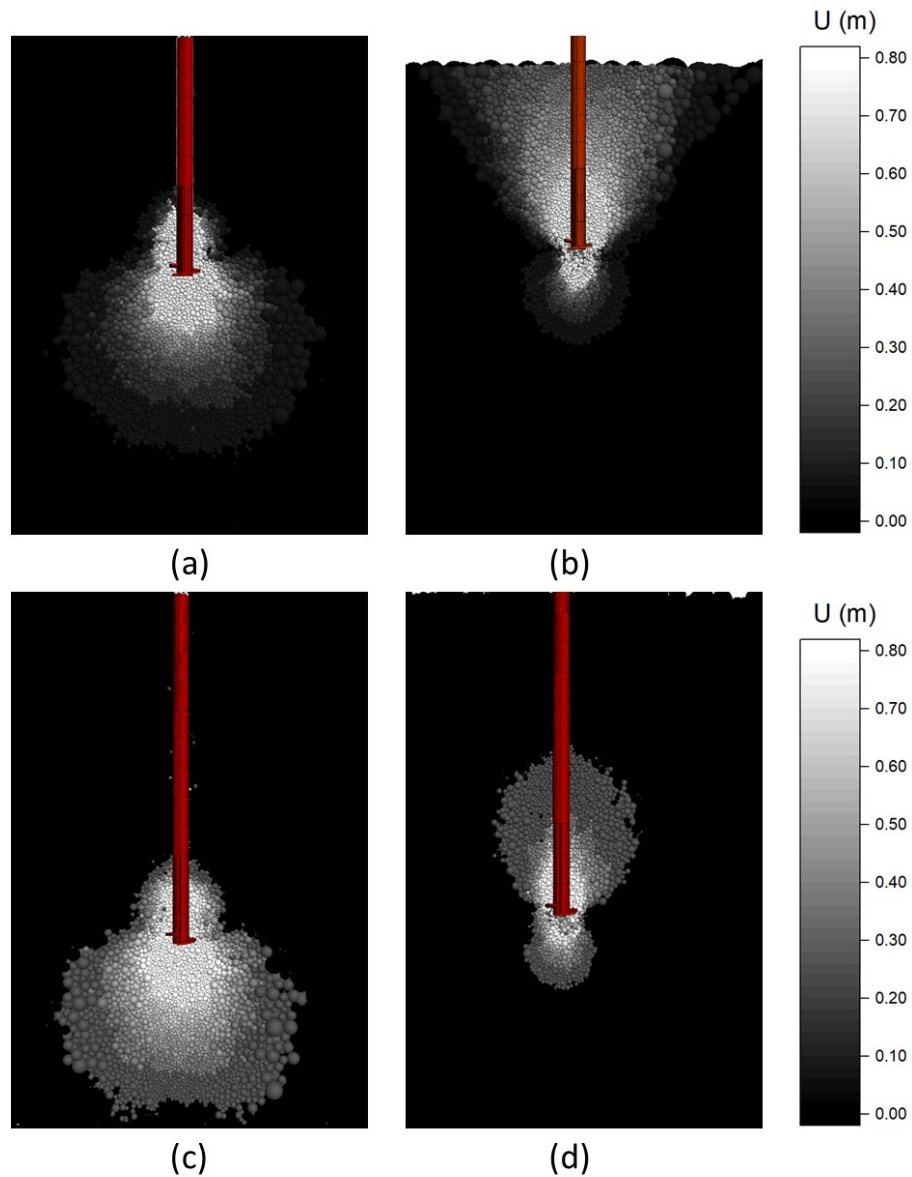


Figure 13: Mechanism form for installed screw piles during axial capacity testing (AR=0.5) a) compression ($H/D_h = 7$) b) tension ($H/D_h = 7$) c) compression ($H/D_h = 11$) d) tension ($H/D_h = 11$)

159x210mm (150 x 150 DPI)

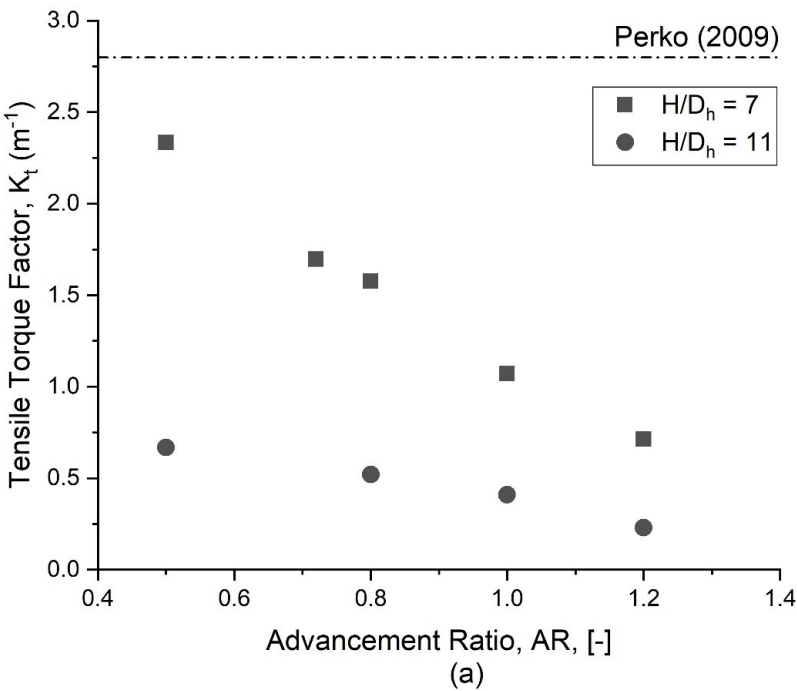


Figure 14: The effect of relative embedment depth and advancement ratio on torque-capacity correlation factors in a dense soil bed. a) Tension b) Compression

149x114mm (220 x 220 DPI)

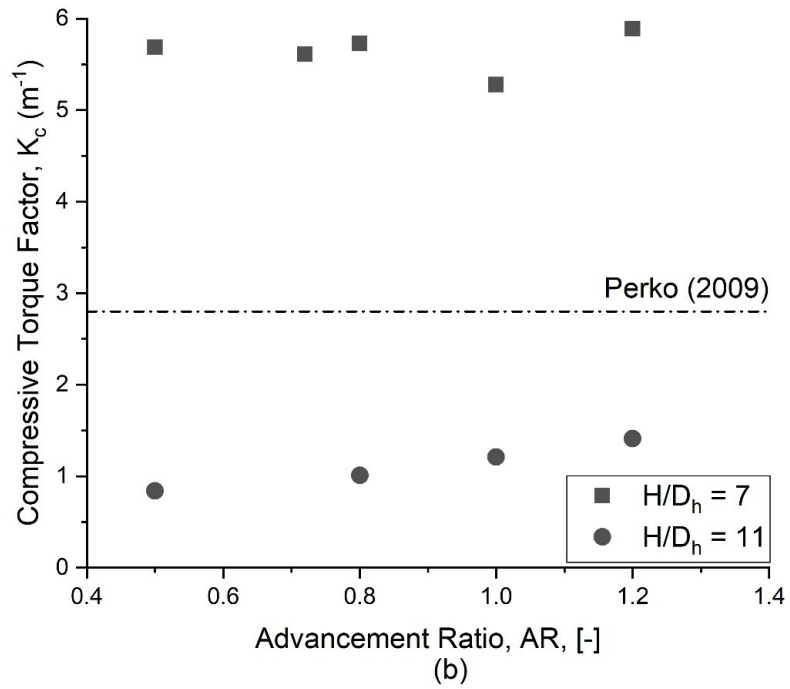


Figure 14: The effect of relative embedment depth and advancement ratio on torque-capacity correlation factors in a dense soil bed. a) Tension b) Compression

149x114mm (220 x 220 DPI)